Prepared for submission to JCAP

Scanning Inflationary Trajectories

J. Richard Bond,[a] **Jonathan Braden,**[a,b] **Andrei V. Frolov,**[c] **Zhiqi Huang**[a] **and Pascal Vaudrevange**[d]

[a]Canadian Institute for Theoretical Astrophysics,
University of Toronto, 60 St. George Street, Toronto, ON, M5S 3H8, Canada
[b]University of Toronto, 60 St. George Street, Toronto, ON, M5S 3H8, Canada
[c]Simon Fraser University, 8888 University Drive, Burnaby, BC, V5A 1S6, Canada
[d]Germany

E-mail: bond@cita.utoronto.ca, jbraden@cita.utoronto.ca, frolov@sfu.ca, zqhuang@cita.utoronto.ca

Abstract. The shapes of the primordial power spectra are the key quantities to unravel the physics of the inflationary epoch. We propose a new framework for parameterizing the spectra of primordial scalar and tensor perturbations, stressing the trajectory nature of the relevant quantities. We show 1) when the data does not contain sufficient information, the reconstructed trajectories, particularly the tensor power spectra strongly depend on the imposed priors and 2) that forthcoming cosmological observations will provide much more information on both scalar and tensor power spectra, allowing the reconstruction of features in the power spectra without imposing strong theoretical priors. Of particular importance is the issue of priors which can be conveniently addressed in this context. Perhaps not surprisingly, the quality of current observational data – despite already providing excellent insights into the cosmological parameters – leaves certain parameters still quite sensitive to the (implied) choice of prior distribution. In particular we find that limits on the tensor scalar ratio r strongly depend on the imposed priors, even leading to an apparent detection of tensor modes in some parameterizations.

Keywords: ...

Contents

1 Introduction

2 Introduction

The cosmic microwave background radiation is a unique window into the physics of energy scales above TeV. Progress towards harvesting its information content has been steady on the experimental side, starting with the COBE experiment [1], continuing with balloon borne experiments such as Boomerang [2], and, most recently, the satellites WMAP [3–6] and

Planck [7]. They delivered a picture of a universe that is extremely homogeneous: Gaussian fluctuations sit on top of a uniform background of photons that stream to us from the surface of last scattering at redshift about 1100, with an amplitude of about 10^{-5}. Decomposing this image of the microwave sky into spherical harmonics shows an angular power spectrum whose features are well understood. Acoustic oscillations in the primordial photon-baryon fluid freeze out at the surface of last scattering, with the photons streaming (almost) freely towards us, showing the familiar acoustic peaks in the angular power spectrum. Their locations and relative amplitudes allow us to infer the energy content of the universe.

Assuming that the inflationary epoch was driven by a scalar field, the absolute amplitude of its scalar power spectrum is directly related to the amplitude of the angular power spectrum.

While experimental advances have been formidable, the exact properties of microscopic theories responsible for the inflationary period remain elusive. A plethora of different scalar field potentials have been suggested, and many of them are compatible with current observations. From a theoretical perspective, the best that can be said is that there are many scalar fields in string theory. As for their potentials, not much is known. Even though some advances have been made in building models of inflation based on or inspired by string theory [8–14], the vast majority of the string landscape is still unchartered.

The usual approach in inflationary model building is to specify parameterized scalar field potentials motivated by fundamental particle physics, proceed to derive the dynamical histories and compare with cosmic observations model by model using only a few parameters such as the scalar amplitude and spectral index, a "top–down" framework. With the increasing emphasis on complex potential landscapes dotted by many local minima with varied structures surrounding them, large ensembles of possible trajectories could arise. Viable trajectories are determined probabilistically, from theoretical "prior" information.

Alternatively, one can take a bottom-up approach from the data, whether with very broad error bars, as in anthropic considerations, or of the increasingly high precision sort offered by the Cosmic Microwave Background (CMB) and Large Scale Structure (LSS) observations. Although there is much art in deciding what theoretical priors to impose, based on concepts such as "baroqueness" of the effective potentials allowed, it is best to allow the priors to be broadly defined and let the data decide what is allowed and what not. It is a well-trod path in concept and one we develop further in this paper.

Traditionally the inflationary dynamics are described in the slow roll approximation, assuming that the inflaton field rolls slowly (or with small acceleration) down its potential. The observables – the primordial tensor and scalar power spectra – can be computed as a function of the slow roll parameters, typically compressed into a restricted set of spectral parameters, such as the scalar amplitude, the tensor-scalar ratio, the scalar power law index, its running and the tensor index. The values of the slow roll parameters, i.e. the parameters of the scalar potential, can thus be inferred using Markov Chain Monte Carlo (MCMC) methods, comparing the model predictions with observations.

In this paper, we advocate a different approach. Instead of starting off with (a family) of scalar field potentials, we aim at reconstructing the shape of the primordial tensor and scalar power spectra independent of theoretical priors (in the sense of expecting certain shapes of the scalar field potential). Instead, we let observational data almost freely decide the shapes of the power spectra, using two different paradigms. The goal is to reconstruct – in a model-independentl way – nontrivial features in the primordial power spectra, if there are any, without imposing strong theoretical priors.

To this end, we consider spectra features produced by some non-standard processes. Examples of such models are particle production during inflation [15, 16], cosmological fluctuations from preheating [17], and "curvaton" models [18, 19]. In these models the consistency relation between tensor and scalar spectra breaks down. We hence let the scalar and tensor spectrum vary independently. In order to generate spectra with a finite number of parameters, we have to impose certain smoothing conditions (priors), implicitly defined by the interpolation method. We vary the interpolation method to show that the dependence on the smoothness prior is weak, provided that proper number of knots are used[1].

Secondly, we consider spectra produced by single-field inflation with exotic features in the potential that can break down the slow roll approximation. Some extreme examples are discussed in e.g. Ref. [20]. For these models we will impose the single field consistency condition, in effect forcing all observables to be derivable from a single real scalar field potential. Once again, we will strive to be agnostic about the shape of the potential. All that we require is an inflationary period.

This paper is structured as follows. Section 3 gives a brief overview of the methods currently discussed in the literature. Sections 6 introduces the different possible parameterizations of background trajectories for the scalar and tensor power spectra without assuming a consistency condition between them. Section 7 discusses the trajectories in the case of inflation driven by a single real scalar field. We summarize our results and conclude in Section 8.

3 Time-dependent observables

When slow roll parameters are sufficiently small so that scale invariance is only mildly broken, a familiar compressed three-dimensional parameter space characterizing the inflation degrees of freedom is appropriate: scalar spectral index n_s, running of the scalar index $n_{\rm run}$ and tensor scalar ratio r. The values are fixed at a given pivot point, a wave number k_p or number of e-folds N_p, typically taken to be about 50 to 60 (or lower, depending on the energy scale of inflation) before the end of inflation. In addition, the overall scalar curvature perturbation amplitude is set at the same pivot point as $\ln A_s = \ln \mathcal{P}_s(k_p)$. A typical pivot point is $k_p = 0.05\,\mathrm{Mpc}^{-1}$. Instead of the tensor amplitude $\ln A_t = \ln \mathcal{P}_t(k_p)$, the scalar tensor ratio $r = \mathcal{P}_t(k_p)/\mathcal{P}_s(k_p)$ is more typically used. For tensors we could add $n_t = d\ln\mathcal{P}_t(k)/d\ln k$ evaluated at k_p as another parameter; however at low order in slow roll, $r = A_t/A_s = -8n_t/(1-n_t/2)$ defines the consistency relation.[2] For this "minimal" set, the scalar power spectrum $\ln \mathcal{P}_s$ is therefore expanded to quadratic order in $\ln k$ while the tensors $\ln \mathcal{P}_t$ are expanded to linear order, but with the linear coefficient for $\ln k$ basically fixed by A_t/A_s.

[1] The criterion is that the reduced χ^2 is not significantly smaller than 1, or expressed in the Bayesian language, the Bayesian evidence is not too low.

[2] There is much to be said for having minimal parameter extensions to explore the data with, building on an adiabatic tilted ΛCDM model characterized by six parameters. Three are associated with abundances, $\omega_b \equiv \Omega_b h^2$, the physical density of baryons; $\omega_c \equiv \Omega_c h^2$, the physical density of cold dark matter; $\theta \equiv 100\ell_s^{-1}$, parameterizing the angular scale ℓ_s^{-1} associated with sound crossing at decoupling, which defines the overall position of the peak–dip pattern and from which the cosmological constant Ω_Λ can be derived. Another is an astrophysical parameter associated with the reionization of the Universe after recombination, τ, the Thomson scattering depth to decoupling. A flat Universe theoretical prior is reasonable to impose on inflation models, the curvature energy $\Omega_k = 1 - \Omega_{tot} \approx 0$. Then there are the two scalar perturbation parameters, $\ln A_s$ and n_s, and, as extensions beyond the basic six, the running scalar index $n_{run} = dn_s/d\ln k$ and r. **super-long footnote is usually very bad-style. Consider change here? – Zhiqi**

3.1 Time evolution of n_s and r

With both n_s and r functions of the wave number k great care must be taken to use the same scale when comparing predictions from model building with observations. Fig. 1 shows the evolution during $\Delta N = 10$ ($N = \int_t^{t_{\rm end}} H dt$ is the number of e-folds before the end of inflation) of n_s and r obtained for an ensemble of randomly generated trajectories using a Chebyshev expansion to order seven (see below). The prior distribution of n_s and r depends on the specific choice of algorithm to generate the inflationary trajectories. For example, if we choose to generate random potentials via interpolation, Fig. 1 will be significantly different. But generically once the slow-roll assumption is given up, n_s and r will be time-dependent. In contrast to this, the observational values for the parameters of the scalar and tensor power spectra are measured at a specific pivot point in k-space, usually taken to be $k_* = 0.05{\rm Mpc}^{-1}$ or $k_* = 0.002{\rm Mpc}^{-1}$, while the values of the logarithmic derivatives of the potential are generically taken at a specific point in time corresponding to a number of e-folds N_* before the end of inflation. In general, the mapping between the number of e-folds and the wave number k depends on the details of the inflationary dynamics and therefore on the parameters of the potential as well as the initial values in case of multiple field models. Also the relation between N and k is altered by the details of preheating after inflation, producing an uncertainty of about 10 in the shift between these two quantities. Taking into account that n_s and r might well be time-dependent quantities, it is obvious that better strategies for relating theory with observations are needed.

3.2 Multifield models

Also, recently there has been a growing interest in models of inflation driven by the combined effect of several scalar fields which arise naturally in the context of e.g. minimal supersymmetric standard model (MSSM) and in string inspired models. With more than one field driving the dynamics, it is not at all clear that there should exist a unique attractor solution to which the trajectories from all initial values of the fields converge. Indeed, there are examples for models with several fields that offer several distinct attractor solutions[21], making the inflationary dynamics heavily dependent on the initial values of the scalar fields.

Major efforts are currently under way to detect the tensor modes in the CMB polarization. This is a challenging signal to observe given the potential foreground contamination of the B-type polarization where a pure tensor contribution is found. A detection of r however is crucial for inflationary model building as it fixes the energy scale of inflation and breaks the degeneracy in the determination of the shape of the underlying potential. So far, the only limits on the energy scale of inflation come from arguments from reheating, while the scalar power spectrum does not provide any information about the energy scale of inflation.

3.3 Trajectory functions

In view of the above we examine in this work a bottom-up approach to model building using the generalized trajectory picture. In our approach, all fundamental quantities such as the tensor and scalar power spectra or slow roll "parameter" ϵ are regarded as trajectories, with a suitable choice of time variable such that there are no ambiguities about the location of observable quantities while at the same time capturing all essential dynamics. Instead of using the traditional parameterization to characterize the primordial power spectra, the trajectory functions are constrained directly using standard parameter estimation packages employing Markov Chain Monte Carlo (MCMC) methods.

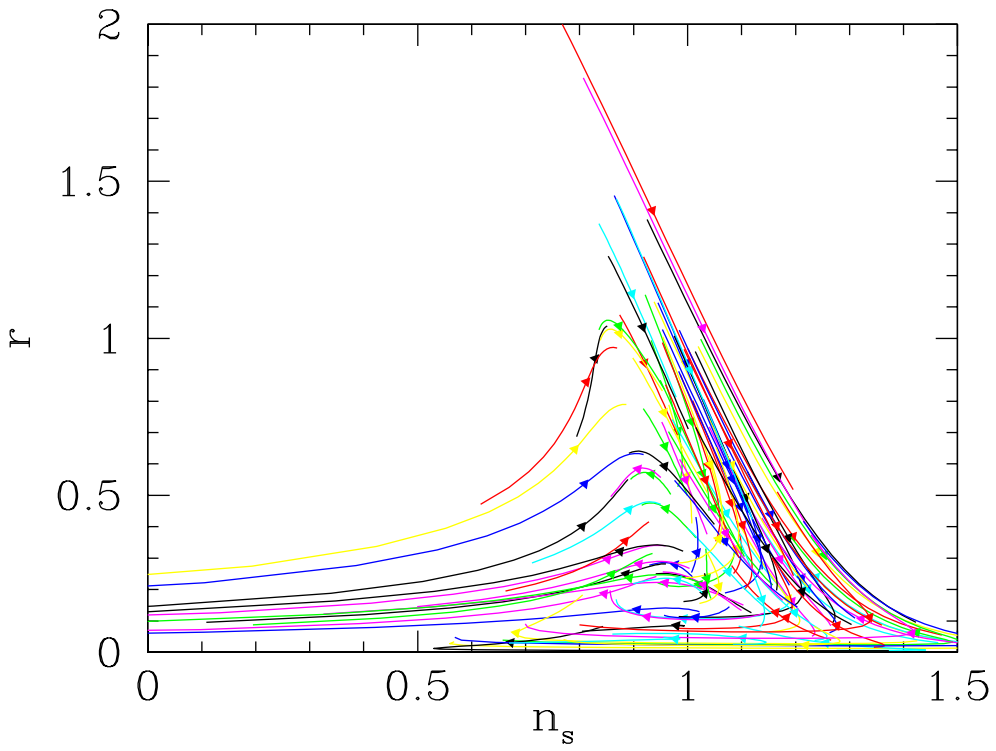

Figure 1. Flow along a random selection of the inflationary trajectories in the n_s *vs.* r plane during 10 e-folds. The trajectories were generated as seventh order Chebyshev expansions of $\epsilon(N)$. Different colors denote different trajectories.

There are many possible choices for the trajectory function, ϵ, $\mathcal{P}_s$, $\mathcal{P}_t$, etc., with the only criterion that one can map the trajectory function to the scalar and tensor power spectra. For example, the trajectory function ϵ encodes all information about single field inflationary models as well as (neglecting the influence of isocurvature perturbations) gentle multiple field model in the sense that a sufficiently well-behaved dynamics can be cast in terms of an effective single field model. Mapping ϵ trajectories to observables requires an integration step. Selecting the power spectra $\mathcal{P}_s$ and $\mathcal{P}_t$ themselves as the trajectory functions offers more flexibility, not only allowing for a non-monotonic tensor power spectrum but also not relying on the single field approximation. In this paper we will focus on the choice of $\mathcal{P}_s$ and $\mathcal{P}_t$ as trajectory functions and also explore the choice of ϵ trajectories.

Different choices of trajectory functions come with different priors. Indeed, as we point out in this work, a discussion of implied priors is integral to this type of bottom-up approach and must be discussed at length. The scalar (tensor) power $\mathcal{P}_s$ ($\mathcal{P}_t$) are constrained to be strictly positive, while ϵ is confined to lie in $\epsilon \in [0, 1]$. Using ϵ trajectories implies single field inflation, a rather complex prior on the allowed trajectories. Furthermore, there is the choice of measure in sampling the chosen trajectories which can be linear or non-linear in the chosen coefficients.

The different priors will sample the functional space of trajectories with different measures. Depending on the quality of observational data this will be reflected in the posterior

space of traditional observables. In particular the value of r is strongly influenced by the choice of trajectory function and the prior distribution of the trajectory values. As we will show, although one can choose a uniform prior in the original expansion coefficients, the mapping through to final parameters is non-trivial and generally results in non-flat priors which in some cases can be quite extreme [22, 23] with a resulting potential for misrepresentation of observational constraints.

When working in this type of bottom-up approach, constraints are imposed directly on the space of trajectories and the traditional parameters become only ancillary products which should not be over interpreted. The focus is shifted instead to the functional reconstruction of the trajectories being considered, $\mathcal{P}_s$ and $\mathcal{P}_t$ in this case. Ultimately the approach can be extended to reconstructing a fundamental trajectory such as $\epsilon(\ln k)$ which leads to direct constraints on the shape of the inflationary potential.

The approach also requires a choice of parameterizing time along the trajectory. A natural choice for this is the wave number k itself. As physical time evolves, modes of decreasing comoving wavelength are stretched outside the horizon, crossing into the super-horizon region when $k = aH$. This leads to the relation $d\ln k = (1-\epsilon)H dt$, where k is the comoving wave number of the mode crossing the horizon, t is the physical time, and $\epsilon = -\frac{\dot{H}}{H^2}$ (where $\dot{H} = \frac{dH}{dt}$) which makes k a good time variable as long as the inflationary stage is not interrupted by periods of non-exponential expansion with $\epsilon \geq 1$.

4 Markov Chain Monte-Carlo

Our Markov Chain Monte Carlo (MCMC) sampler is based on the publicly available `COSMOMC` [24] and allows us to obtain posterior distributions for the power spectra parameters as well as the remaining background cosmological parameters. The first three are related to abundances: $\omega_b \equiv \Omega_b h^2$, the physical density of baryons, $\omega_c \equiv \Omega_c h^2$, the physical density of cold dark matter, and $\theta \equiv 100\ell_s^{-1}$, parameterizing the angular scale ℓ_s^{-1} associated with sound crossing at decoupling, which defines the overall position of the peak–dip pattern and from which the cosmological constant Ω_Λ can be derived. The remaining parameter, τ, sets the amount of reionization of the universe after recombination in the form of Thomson scattering depth to decoupling. A flat universe theoretical prior is reasonable to impose on inflation models, with the curvature energy $\Omega_k = 1 - \Omega_{\rm tot} \approx 0$.

There are data constraints beyond the CMB and LSS regions that are only loosely determined, i.e. "weak" prior probabilities, informed by broad brush stroke considerations, but still quite limiting. One is that the Universe underwent significant inflation, translating at lowest order to $0 < r < 16$ over the entire k range within the horizon. For the dynamical trajectories this corresponds to $0 < \epsilon < 1$, or equivalently an inflationary period that lasted for a sufficient number of e-folds N.

Enough inflation implies that scales of topological structures cannot be too small so that there is sufficient cosmic complexity to give rise to life. Also, the amplitude of the power spectrum at high k cannot be too large otherwise surviving primordial black holes (PBH) formed in abundance. Another weak prior driven by the CMB data is that the Compton "optical" depth cannot be too large or else there would be no CMB fluctuations on small scales. This reflects in the formation of the first ionizing stars and is more strongly restrictive than the PBH constraint. The epoch of galaxy formation is also a constraint, often used in a very broad way in anthropic arguments. The data on high redshift galaxy abundances has

Table 1. The 68.3% CL constraints on cosmological parameters (for r the 68.3%CL and 95.4% CL upperbounds are shown). A ΛCDM model with $n_t = 0$ has been assumed. For simplicity we have used the same pivot $k_{\rm pivot} = 0.002\,{\rm Mpc}^{-1}$ for both scalar and tensor spectra. The data sets used here are described in Section 6.

	with $n_{\rm run}$	without $n_{\rm run}$
$\Omega_b h^2$	$0.02262^{+0.00043}_{-0.00044}$	$0.02260^{+0.00044}_{-0.00044}$
$\Omega_c h^2$	$0.1179^{+0.0020}_{-0.0020}$	$0.1171^{+0.0019}_{-0.0019}$
θ	$1.0425^{+0.0019}_{-0.0020}$	$1.0420^{+0.0019}_{-0.0019}$
τ	$0.094^{+0.015}_{-0.014}$	$0.090^{+0.014}_{-0.014}$
n_s	$1.006^{+0.029}_{-0.029}$	$0.962^{+0.011}_{-0.011}$
$n_{\rm run}$	$-0.017^{+0.010}_{-0.010}$	...
$\ln(10^{10} A_s)$	$3.184^{+0.043}_{-0.047}$	$3.226^{+0.033}_{-0.034}$
r	$0.0000^{+0.14+0.27}$	$0.0000^{+0.08+0.17}$
Ω_m	$0.293^{+0.012}_{-0.011}$	$0.290^{+0.011}_{-0.010}$
σ_8	$0.844^{+0.014}_{-0.014}$	$0.843^{+0.014}_{-0.016}$
$z_{\rm re}$	$11.2^{+1.2}_{-1.2}$	$10.8^{+1.2}_{-1.2}$
H_0	$69.3^{+1.0}_{-1.0}$	$69.4^{+1.0}_{-1.0}$

improved enormously in recent years and even with the uncertainties associated with gas and radiation at early times can significantly constrain the power spectrum.

Improved observations narrow down the range of allowed variations. In the eighties, upper limits on CMB fluctuations combined with a few LSS constraints already restricted the allowed possibilities. The COBE data further restricted what was allowed, and now in the era of WMAP and higher resolution experiments, the possibilities for significant variation from the standard model are much more limited.

Using the traditional parameterizations of the primordial power spectra in terms of A_s and n_s and the most current data including weak lensing, supernova and Lyman-α forest (see Section 5), current constraints on the basic 6-parameter model are given in Table 1, most notably $n_s = 0.962^{+0.011}_{-0.011}$. Including either r or $n_{\rm run}$, we find $r < 0.17$ at the 95% confidence limit with $n_{\rm run} = 0$ and $r < 0.27$ with $n_{\rm run} = -0.017^{+0.010}_{-0.010}$. Here we consider the two parameter r and $dn_s/d\ln k$ extension to the base model.

5 Data Sets

Before we proceed, we give a brief overview over the data sets that we use in this paper. Besides current data sets, we also elaborate on forecasts for future experiments.

- *Cosmic Microwave Background (CMB)*

  Our complete CMB data sets include WMAP-7yr [6, 25], ACT [26], BICEP [27], QUaD [28], ACBAR [29–32], CBI [33–36], BOOMERANG [37–39], VSA [40], and MAXIMA [41]. For high-ell CMB experiments we have used the Sunyaev-Zel'dovich (SZ) secondary anisotropy [42, 43] template [44], but other choices of SZ template are certainly possible [45–47]. We treat the multiplier of the SZ template as a free nuisance parameter $A_{\rm SZ}$ and marginalize over it, making the cosmological parameters insensitive to the choice of SZ template. The CMB lensing contribution is included when we calculate CMB power spectra.

Table 2. Weak Lensing Data Sets

Data sets	$A_{\rm eff}$ (deg^2)	$n_{\rm eff}$ (arcmin^{-2})
COSMOS[57, 58]	1.6	40
CFHTLS-wide[59, 60]	22	12
GaBODS[61, 62]	13	12.5
RCS[61, 62]	53	8
VIRMOS-DESCART[60, 63]	8.5	15

- *Type Ia Supernova (SN)*

  We use the [48] data set, which have combined the SDSS-II SN samples with the data from the ESSENCE project [49, 50], the Supernova Legacy Survey (SNLS) [51], the Hubble Space Telescope (HST) [52–55], and a compilation of nearby SN measurements. Two light curve fitting methods, MLCS2K2 and SALT-II, are employed in [48]. The different assumptions about the nature of the SN color variation lead to a significant discrepancy in dark energy parameters. Since we are only interested in primordial power spectra and assuming a cosmological constant, our choice of SALT-II filter throughoutt this paper does not have significant impact on our results.

- *Large Scale Structure (LSS)*

  The LSS data used in this paper is the power spectrum of the Sloan Digital Sky Survey Data Release 7 (SDSS-DR7) Luminous Red Galaxy (LRG) samples [56].

- *Weak Lensing (WL)*

  Five WL data sets are used in this paper. The effective survey area $A_{\rm eff}$ and galaxy number density $n_{\rm eff}$ of each survey are listed in Table 2.

  For the COSMOS data, we use the CosmoMC plug-in written by Julien Lesgourgues [58]. For the other four weak lensing data sets we use the covariance matrices given by Benjamin *et al.* [64]. To calculate the likelihood we wrote a CosmoMC plug-in code. We take the best fit parameters α, β, z_0 for $n(z) \propto (z/z_0)^\alpha \exp\left[-(z/z_0)^\beta\right]$, and marginalize over z_0, assuming a Gaussian prior with a width such that the mean redshift z_m has an uncertainty of $0.03(1+z_m)$. We have checked that further marginalizing over the remaining $n(z)$ parameters α and β has no significant impact [65, 66]. We use the Halofit formula [67] to map the linear matter power spectrum to nonlinear power spectrum. Because we are considering non-standard forms of primordial spectra, the Halofit formula can be inaccurate , potentially washing out bump features by non-linear dynamics). To model this additional uncertainty, we introduce two nuisance parameters α_h and β_h

$$\ln P_{\rm nl} = e^{-k^2 r_{\rm nl}^2} \ln P_{\rm halofit} + \left(1 - e^{-k^2 r_{\rm nl}^2}\right) \times \left(\ln P_{\rm smooth} + \alpha_h + \beta_h k r_{\rm nl}\right) \ , \tag{5.1}$$

  where $P_{\rm halofit}$ is calculated using the original halofit formula code, with the nonlinear scale $r_{\rm nl}$ as a byproduct. Here $\ln P_{\rm smooth}$ is obtained by fitting $\ln P_{\rm halofit}$ as a quadratic function of $\ln k$ in the range where $\ln(k r_{\rm nl}) > -1$ and $k < {\rm Mpc}^{-1}$. We used priors $-0.2 < \alpha_h < 0.2$ and $-0.2 < \beta_h < 0.2$, allowing about 20% uncertainty of $P_{\rm nl}$ on scales

$\sim 1/r_{\rm nl}$, and even larger uncertainties on smaller scales. By doing this we are effectively discarding most of the information on non-linear scales, with only a rough amplitude of the matter power spectrum being used.

- *Lyman-α Forest (Lyα)*

  We use Lyα data sets given in McDonald *et al.* [68, 69]. To calculate the likelihood, we interpolate the χ^2 table in a three dimensional parameter space, where the three parameters are amplitude, index, and the running of linear matter power spectrum at pivot point $k_{\rm lya} = 0.9h$ Mpc^{-1}. To extract these parameters from more general power spectra that are allowed in our parametrization, we perform a quadratic fitting of $\ln P_{\rm matter}$ for $\ln k_{\rm lya} - 1/2 < \ln k < \ln k_{\rm lya} + 1/2$, and marginalize over 2% uncertainty of the amplitude and 5% uncertainty of the spectral index.

In addition to the most current catalog of cosmological data sets, we consider in alternatively forcast data from forthcoming cosmic surveys. The Planck satellite is expected to measure the CMB temperature fluctuations to ultimate accuracy [70]. The EUCLID weak lensing survey will probe large scale structure deep into redshift 1.1 [71], with possible extensiosn to much higher redshift by 21-cm surveys such as the Canadian Hydrogen Intensity Mapping Experiment (CHIME) [72]. The Joint Dark Energy Mission (JDEM) will expand the current supernova catalog by an order of magnitude [73]. To model these forthcoming data sets, we assume that the mapping between linear and nonlinear matter power spectra is well understood (especially for the more general power spectra we consider here). We hence directly apply the likelihood codes and mock data simulation techniques that we used in Ref. [66], with no further modifications for more general primordial spectra.

6 Spectral Trajectories

As indicated in the introduction, we will first focus on the reconstruction of the primordial power spectra while ignoring any priors from mechanisms that would produce them. Specifically in this section, we shall not assume a scalar field driving inflation, i.e. the consistency condition between the scalar and tensor perturbation spectra. Instead we vary the $\mathcal{P}_t, \mathcal{P}_s$ (or some quantities related to them) as independent spectral trajectory functions. Only observational data can and shall decide whether a trajectory is permissible or not.

The power spectra are traditionally parameterized as

$$\mathcal{P}_t = A_t \left(\frac{k}{k_p}\right)^{n_t} , \quad \mathcal{P}_s = A_s \left(\frac{k}{k_p}\right)^{n_s - 1} , \tag{6.1}$$

where $A_{t,s}$ are the tensor and scalar amplitudes, and $n_{t,s}$ are the corresponding spectral indices which are generally assumed to be constant. Common values for the position of the pivot point k_p are $0.05\,\mathrm{Mpc}^{-1}$ and $0.002\,\mathrm{Mpc}^{-1}$. In this language, the consistency relation is $n_t = -\frac{\mathcal{P}_t}{8\mathcal{P}_s}$. Figure 2 shows the limits on the values of the tensor scalar ratio $r \equiv \frac{\mathcal{P}_T}{\mathcal{P}_S}$ and the scalar spectral index n_s.

From a theoretical point of view, the running of the spectral index can generally be non-zero, $n_{\rm run} = \frac{dn_s}{d\ln k} \neq 0$. Although recent observations do not see a significant probability for non-zero running, one has to keep in mind that this result could possibly be driven by an implicit prior in the choice of parameterization. Different parameterizations might not conclusively detect non-zero running, but they can show that the bounds on $|n_{\rm run}|$ are larger than the standard parameterization suggests.

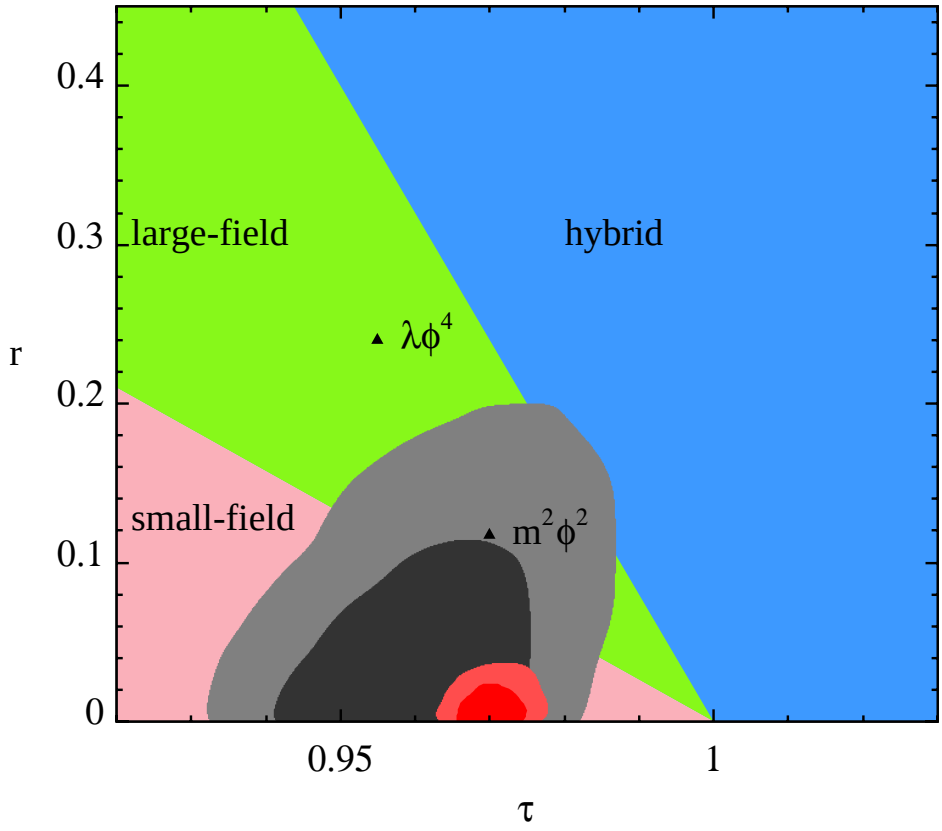

Figure 2. Limits on the values of the tensor scalar ratio r and scalar spectral index n_s for current data (grey contours) as well as a forecast for Planck (red contours). Also displayed are the different classes of single scalar field theories covering this space of observables. Here $n_{\rm run} = 0$ and $n_t = 0$ are assumed.

The traditional parameterization of the power spectra with a constant n_s is motivated by the fact that a pure deSitter stage of inflation has perfectly flat power spectra and that in many models of inflation driven by a scalar field, the field is almost constant during inflation, producing fluctuations with n_s only slightly different from unity. But these considerations are just a theoretical bias. Observational data should be determining the parameters of the primordial power spectra as unbiased as possible.

We will expand the trajectory function $f(x) = \mathcal{P}_{S,T}$ in terms of basis functions w_i

$$f(x) = \sum_i f_i w_i(x)\,, \tag{6.2}$$

where the functions $w_i(x)$ are either Chebyshev polynomials, a suitable representation of B-splines or Hermite polynomials (see Appendix A for more details and a brief introduction to both). By using high order expansions, we explore the freedom that is in the data, while at the same time we shall keep an eye on the effect of priors.

The trajectory functions are subject to certain constraints, such as positivity for the power spectra, or being confined in the interval $[0, 1]$ for the slow roll parameter ϵ. Sampling the coefficients and then rejecting the trajectories that do not fulfill the constraints is both

inefficient and – more severely – implies a prior on the coefficients that is hard to overcome. Thus, the values of the trajectories at the knots of the expansion should be sampled.

As we will see below, even this approach has some disadvantages. If the data is not strong enough, the reconstructed trajectories might show oscillatory features, or some residual implicit prior , e.g. positivity, might induce spurious detection of the tensor power spectrum. As it is known beforehand that the currently available observations do not possess enough power to constrain the tensors, we shall parameterize $\mathcal{P}_t$ at most by the tensor scalar ration r and a tensor index n_t.

As observational data is only available from the horizon size up to the scale of Lyman-α clouds, we restrict the range in k-space over which to expand the trajectories to $-9 < \ln\left(k/\mathrm{Mpc}^{-1}\right) < 1$.

6.1 Interpolation between seven knots

First, we will discuss our results for a semi-blind expansion of $\ln \mathcal{P}_s$ using natural cubic spline interpolation between 7 knots while parameterizing the tensor spectrum using A_t and n_t (with priors $A_t > 0$ and $-0.1 < n_t < 0$).

6.1.1 Results for current data

Figure 3 shows the best-fit scalar (solid blue) and tensor (solid red) power spectra together with trajectories from within a 1-σ interval around the best-fit points (shown in dashed blue/orange). While the tensor power spectrum is largely unconstrained with $r(0.002\,\mathrm{Mpc}^{-1}) < 0.89$ at 95.4% CL, the scalar power spectrum is somewhat better constrained – which will have profound implications for the spurious detection gravitational waves when taking into account the consistency condition for single field inflation below. However, the scalar spectrum is only well constrained within the range $0.002\,\mathrm{Mpc}^{-1} \lesssim k \lesssim 0.1\,\mathrm{Mpc}^{-1}$, due to the presence of cosmic variance on large scales and nonlinear structures on small scales.

As can be seen in Figure 5, the response of the C_ℓ's to the reconstructed primordial power spectra is consistent with the uncertainties of the measured CMB angular power spectra (including cosmic variance). Panel Figure 5(a) shows the best-fit angular temperature autocorrelation function in solid red, and trajectories from within a 1σ interval around the best fit points in dashed blue. While on scales $\ell > 20$, there is only a small uncertainty in the scalar power spectrum, cosmic variance leaves the angular scales $\ell < 20$ rather unconstrained, with strong deviations from the best fit trajectory possible. Note that these wild excursions of the scalar power cannot be seen when parameterizing $\mathcal{P}_s$ with only an amplitude and a spectral index: In this case, the constraints from scales $0.002\,\mathrm{Mpc}^{-1} \lesssim k \lesssim 0.1\,\mathrm{Mpc}^{-1}$ fix the local slope of the spectrum quite tightly. On the other hand, the increased freedom of the trajectories – especially with larger number of nodal points – enables much stronger features in $\mathcal{P}_s$.

Panel 5(b) shows the B-mode polarization. As expected, the contribution to the C_ℓ^{BB} spectrum coming from the primordial tensors (shown in solid black and dashed green) is completely unconstrained from below and shows no signs of an unambiguous detection.

6.1.2 Principal Component Analysis

Recently, principal component analysis (PCA, [74]) has gained some attention [75]. This is another way of representing trajectories, however not as an expansion in a fixed set of basis functions. Instead, the basis functions vary depending on the error bars of the data.

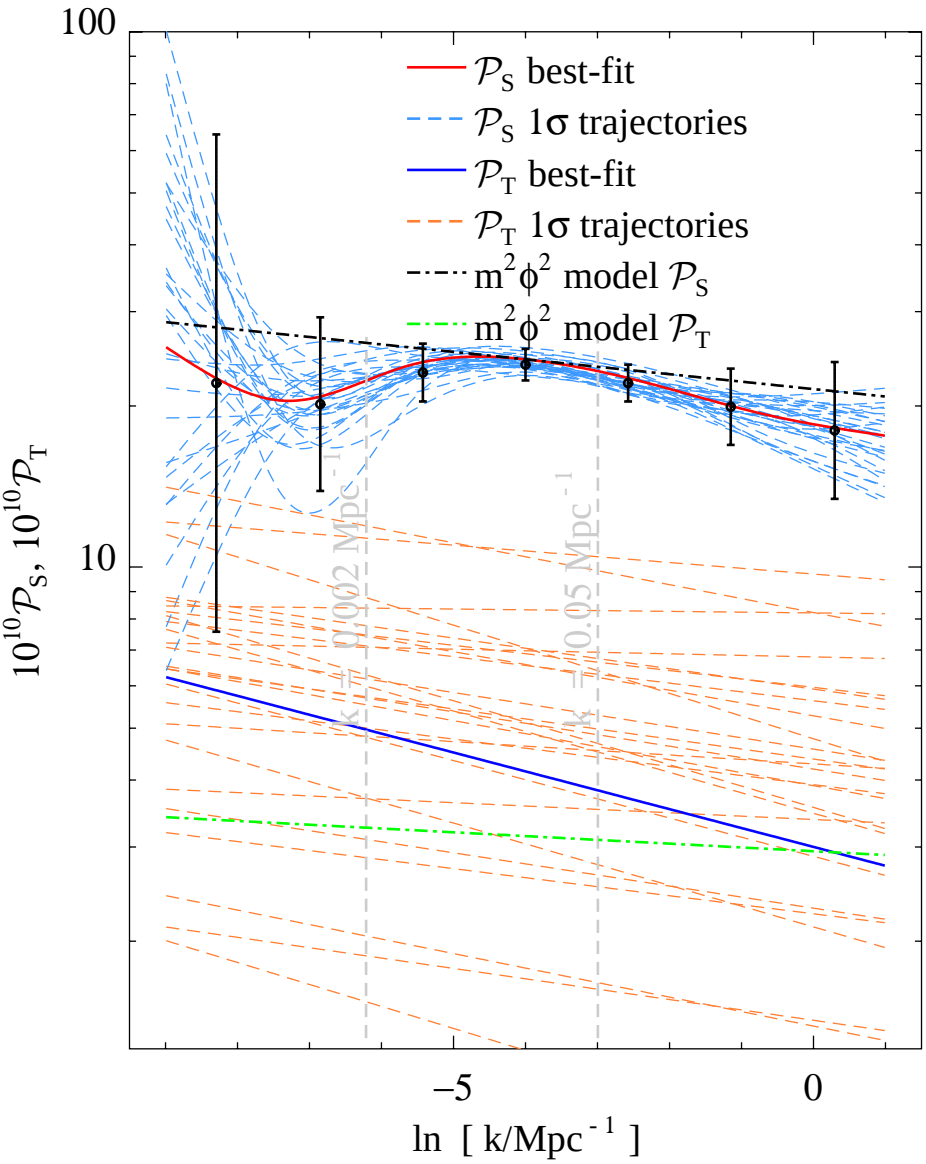

Figure 3. Reconstructed best fit scalar (solid red) and tensor (solid blue) power spectra using the current data. Also shown are the band powers obtained by convolving the power spectra with top-hat window functions in uniform $\ln k$ bins, with black error bars representing the 1σ uncertainties and correlation matrix shown in Figure 4. Trajectories from the 1σ interval around the best-fit points are shown as dashed blue and dashed orange lines for the scalars and tensors, respectively. The power spectra for $m^2\phi^2$ (dot-dashed black line for scalar and dot-dashed green line for tensor) agree pretty well with the reconstructed scalar spectra. The logarithm of the scalar spectrum was interpolated in cubic splines between 7 uniformly distributed $\ln k$ knots whereas the tensor spectrum was parameterized as $A_t\,(k/k_{\rm pivot})^{n_t}$ with prior $-0.1 < n_t < 0$. At 95.4%CL, $r(0.002\,{\rm Mpc}^{-1}) < 0.89$.

They are determined as the eigenfunctions of the covariance matrix of either the observable data points themselves or some derived quantities. So while in intermediate steps, the trajectories under consideration are still expanded in basis functions, the final results are represented as the eigenmodes of their coefficients' covariance matrix, with only the best-

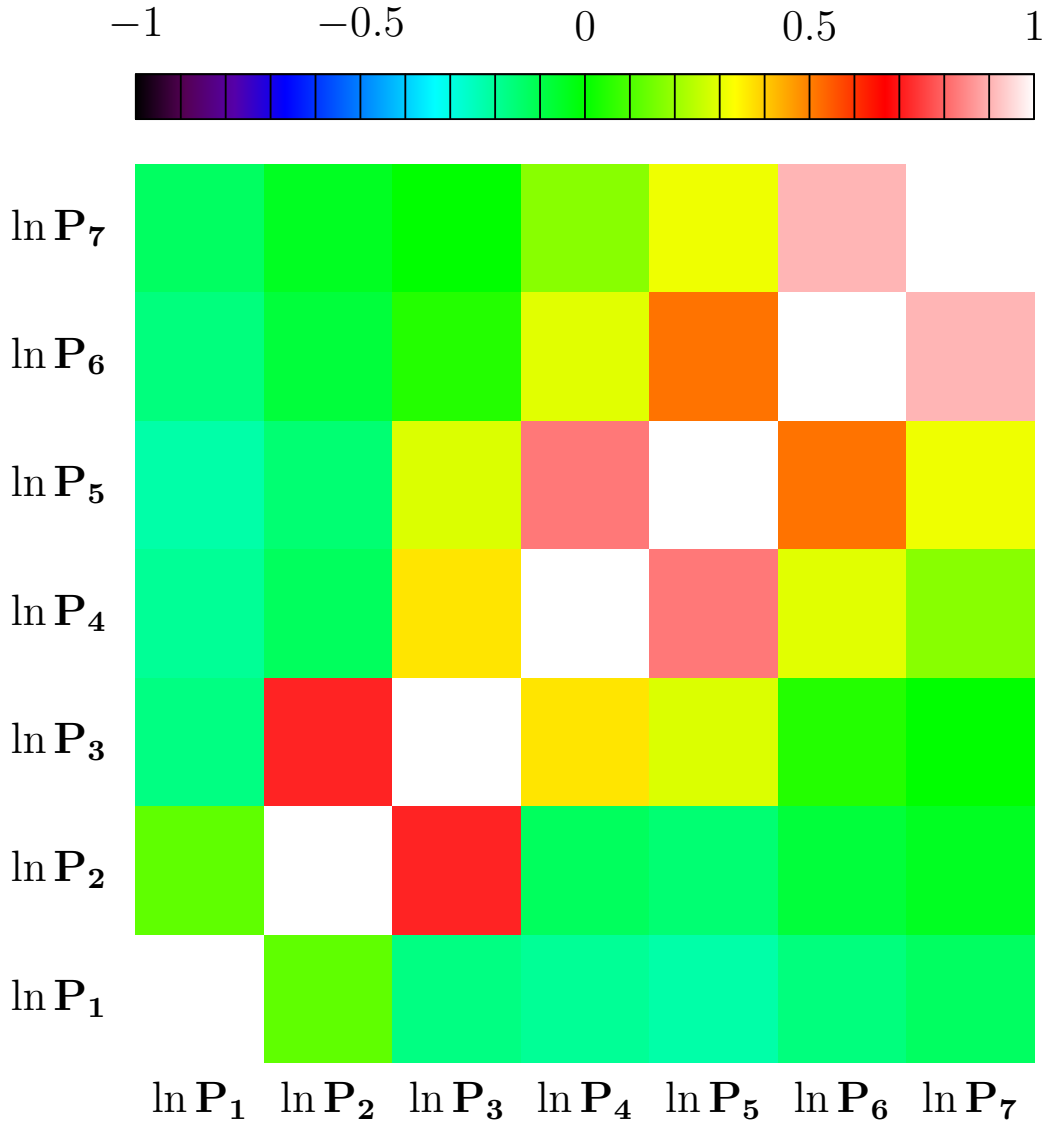

Figure 4. Correlation matrix of the reconstructed scalar power spectrum (see Figure 3). The neighboring band powers are strongly correlated whereas those far away have almost no correlation.

constrained eigenmodes kept for analysis. In Figure 6 we show the eigenmodes of a 10 knot cubic spline interpolation of $1 - n_s$. After constraining the values of the trajectories at the knots and obtaining their covariance matrix, we diagonalize this matrix and only display the first three eigenmodes which have eigenvalues $0.015^2, 0.017^2, 0.032^2$. They are peaked around $\ln \frac{k}{\mathrm{Mpc}^{-1}} = -3.8, -4.5$, and $-2.5\,\mathrm{Mpc}^{-1}$, corresponding to $\ell = 160, 80, 580$. **The first eigen mode is close to a single peak, $\ell = 160$ (close to the first CMB peak) makes sense. The second and third eigen modes have multiple peaks. We should probably not say they are peaked around some ℓ. – Zhiqi**

Alternatively, one might perform this eigenmode analysis for all other trajectory expansions. However, the bottom line is that the PCA – while providing a useful measure of the amount of information in the data – does obscure the influence of priors, something that is

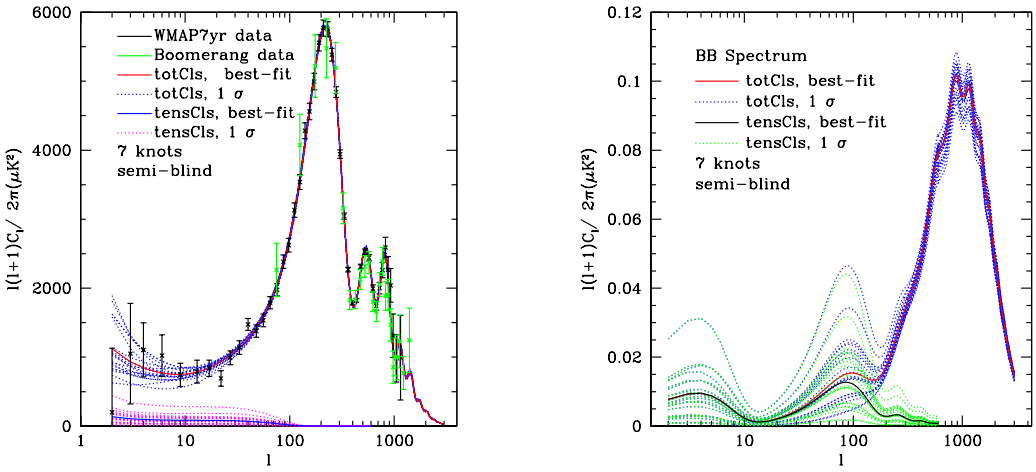

(a) (b)

Figure 5. Response of the angular power spectrum C_ℓ for (a) temperature (TT) anisotropies and (b) B-mode polarization. The best fit trajectories are shown in solid red, while sample trajectories from within a 1σ interval around the best fit point are shown in dashed blue. Panel (a) shows the best fit contribution of the tensors to the TT spectrum in solid black as well as its 1σ variation (in dashed purple).

much more readily visible in the trajectory approach.

6.1.3 Results for forecasts

In parallel we discuss forecasting future experiments using the freely varying $\mathcal{P}_s, \mathcal{P}_t$ trajectories. Besides the interest in forecasts in their own right, this also serves as a further exercise that shall convince us that we did not introduce any serious bugs into CosmoMC. We will examine two different fiducial models, both with the same fiducial amplitude and scalar spectral index $n_s = 0.97$, but different in tensor scalar ratio r.

First, we reconstruct the inflationary trajectories $\mathcal{P}_s, \mathcal{P}_t$ for a fiducial $V(\phi) = m^2\phi^2$ model of inflation, with a tensor scalar ratio $r(0.002\,\mathrm{Mpc}^{-1}) = 0.13$, see Figure 7(a). The scalar perturbations are well recovered: the solid red best fit trajectory and the dashed blue 1σ trajectories fit nicely to the dashed dotted black fiducial $\mathcal{P}_s$. The fiducial amplitude of the tensors (shown in dashed dotted green) is found with about 1σ precision. However the slope of the tensors n_t seems quite off, and essentially is driven by the chosen prior $-0.1 < n_t < 0$. Even with data sets that will be available in the near future, the tensor spectral index will not be constrained. Only experiments like the big bang observer (BBO) will be able to shed more light on the shape of the tensor power spectrum.

Secondly, we reconstruct a fiducial model with $r = 0$ in Figure 7(b). Again, the scalar spectrum is beautifully recovered. Only an upper limit on the tensors is found, consistent with $r = 0$. To test the dependence of our results of the choice of interpolation method, in Figure 7(b) we have used a different interpolation method – the monotonic cubic Hermite

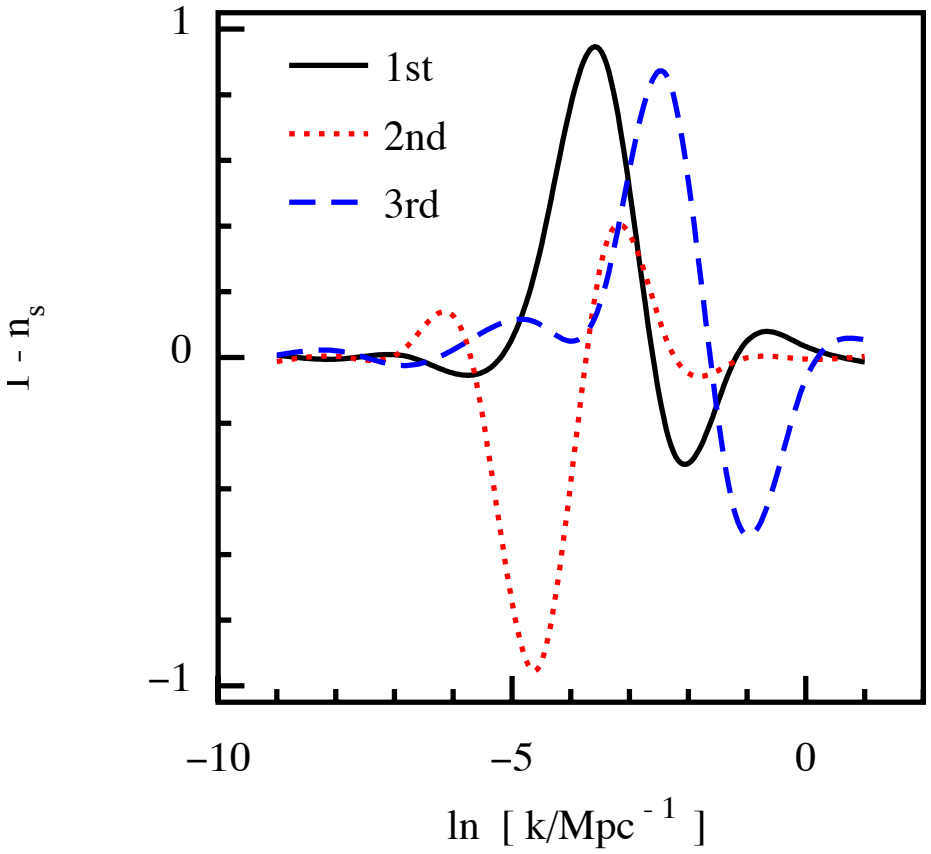

Figure 6. The first (solid black), second (dot red) and third (dashed blue) eigen modes of $1 - n_s$. Here we have done natural cubic spline interpolations of $2\epsilon + d\ln\epsilon/d\ln k \approx 1 - n_s$ between 10 knots, assuming single-field inflation.

interpolation. The technical details of various interpolation methods we employed are given in the Appendix.

6.2 Effects of changing the details of the trajectory expansion

While the reconstructed power spectra do not differ much when using monotonic cubic Hermite interpolation (or an expansion Chebyshev polynomials) instead of cubic splines, varying the priors results in dramatic changes in the power spectra. Priors can be changed either explicitly (e.g. assuming a uniform prior in $\ln A_t$ instead of A_t) or implicitly (by sampling the coefficients of the spline/ Chebyshev expansion instead of the trajectory values at the knots). The effects of changing the priors explicitly are rather trivial. For example, a uniform prior in $\ln A_t$ leads to much tighter upper limit on the tensor spectrum. Other changes to the details of the trajectory expansions are more subtle. We will discuss some notable examples in the following.

6.2.1 Connection to the standard parameterization

In order to connect our work to the standard parameterization, we performed an order 2 natural cubic spline expansion (i.e. linear interpolation) for $\ln \mathcal{P}_s$ which has the same number

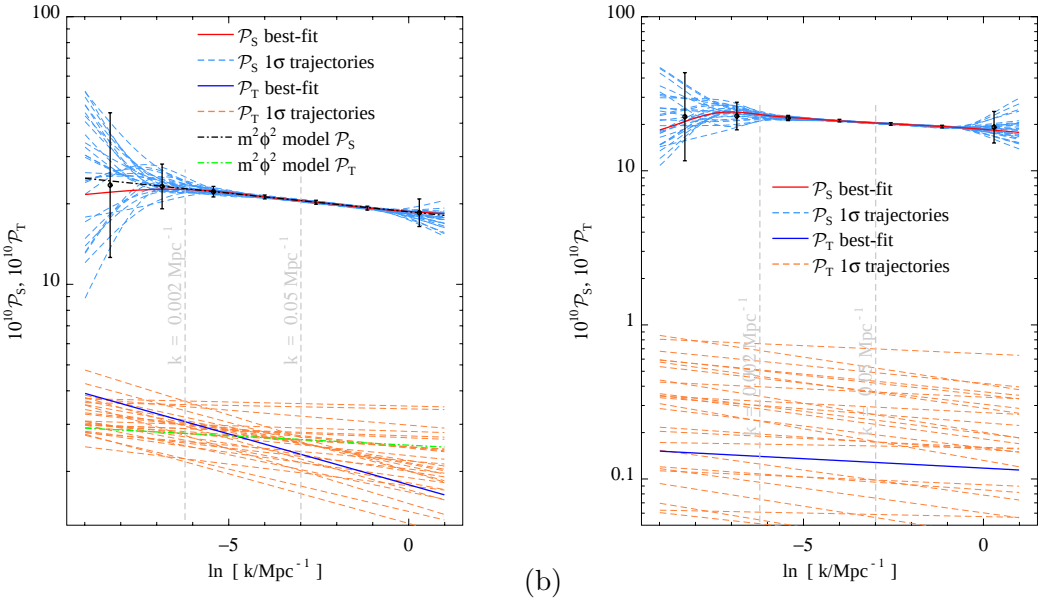

Figure 7. Reconstruction of (a) the fiducial $m^2\phi^2$ inflationary model with $r = 0.13$ and (b) a fiducial model with $r = 0$, assuming 2.5 years of Planck data. The solid red/ dashed blue line shows the best fit/ 1σ $\mathcal{P}_s$ trajectories. The solid blue/ dashed red line shows the best fit/ 1σ $\mathcal{P}_t$ trajectory. The scalars/ tensors of the fiducial model in (a) are shown as dashed dotted black/ green line. For both models, the $\mathcal{P}_s$ reconstruction works spectacularly well. In (a), the reconstructed amplitude of $\mathcal{P}_t$ agrees within errors bars, however the slope seems quite off. The logarithm of scalar spectrum was interpolated in cubic splines (panel (a)) or cubic hermite (panel (b)) between 7 uniformly distributed $\ln k$ knots. The tensor spectrum was parameterized as $A_t\,(k/k_{\rm pivot})^{n_t}$ with prior $-0.1 < n_t < 0$.

of degrees of freedom as the standard parameterization using $\ln A_s, n_s$. It is trivial to convert the values of $\ln \mathcal{P}_s$ at the 2 knots to $\ln A_s, n_s$. Figure 8 shows the reconstructed primordial trajectories for $\mathcal{P}_s$ trajectory with 2 knots, employing the same color code as Figure 3. Not surprisingly, the resulting values for $\ln\left(10^{10}A_s\right) = 3.220^{+0.037}_{-0.036}$, $n_s = 0.966^{+0.011}_{-0.012}$ are in excellent agreement with the values obtained by the standard parameterization (with $r > 0$ and $-0.1 < n_t < 0$) $\ln\left(10^{10}A_s^{\rm std}\right) = 3.226^{+0.033}_{-0.034}, n_s^{\rm std} = 0.962^{+0.011}_{-0.011}$. The small differences come from a slight change in priors due to the different parameterizations.

6.2.2 Oscillations from too much freedom

Having made the connection with the standard parameterization by employing a 2-knot natural cubic spline, we now examine the effects of allowing more freedom for the scalar spectrum. As example we will use a 11-knot cubic spline expansion for $\ln \mathcal{P}_s$. In Figure 9, we see the presence of oscillatory features, particularly on scales where $\mathcal{P}_s$ is not well determined. They are due to an excessive number of degrees of freedom in the parametrization. However, when mapped into C_ℓ space, the resulting angular power spectra agree with observations within (cosmic variance-dominated) error bars.

6.2.3 Tensor power spectrum driven by prior

As a final example of the effects of different priors, we take a look at the impact of increasing the number of knots for the tensor power spectrum interpolation. The monotocity condition $d\ln\mathcal{P}_t/d\ln k < 0$ required by inflation is applied to the $\mathcal{P}_t$ trajectories. Figure 10 shows that

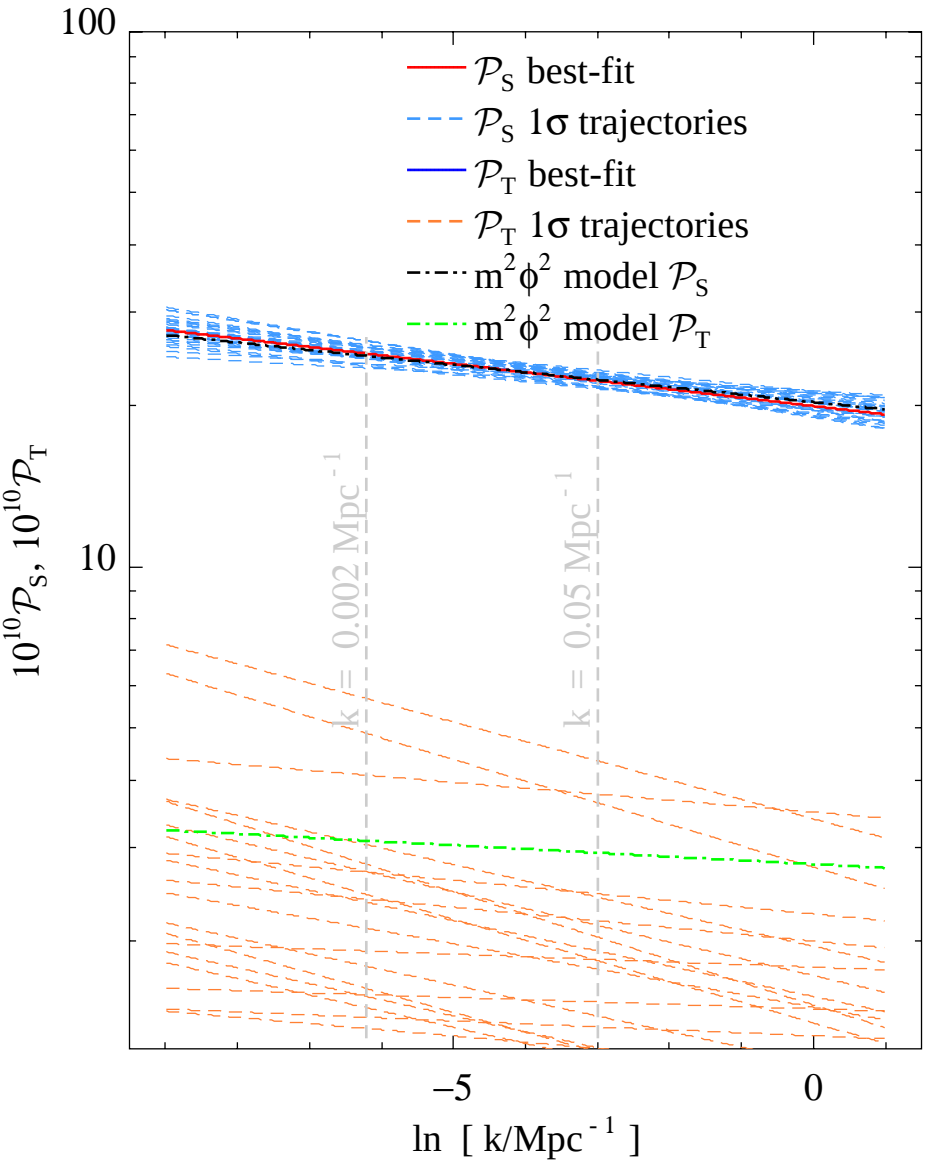

Figure 8. The reconstructed scalar and tensor power spectrum, using natural cubic splines with 2 nodal points for $\mathcal{P}_s$ and r, n_t (with priors $r > 0$ and $-0.1 < n_t < 0$) for $\mathcal{P}_t$.

an increase in the allowed complexity for the tensor (from 2 degrees of freedom to 5) leads to detection of $\mathcal{P}_t$ on large scales. This detection is known to be false, because the fiducial model has $r = 0$. The favored larger amplitude of $\mathcal{P}_t$ on large scales is driven by the monotonicity prior, as clearly visualized in the figure.

Alternatively, one can easily see the influence of the prior on the reconstructed parameters when simulating data for a Planck or CMBPol type experiment, see Figure 11. Reconstructing the input values $r_{\rm reconstructed}$ of the input tensor scalar ration $r_{\rm in}$ shows that for at the limits of the experiment – for small enough values of $r_{\rm in}$, e.g. $r_{\rm in} = 0.0001$ for CMBPol – the priors drive the reconstructed value. While for the $\mathcal{P}_s, \mathcal{P}_t$ trajectory (black) the reconstructed value $r_{\rm reconstructed}$ is too large, in the case of an ϵ (red) or $\ln \epsilon$ (blue)

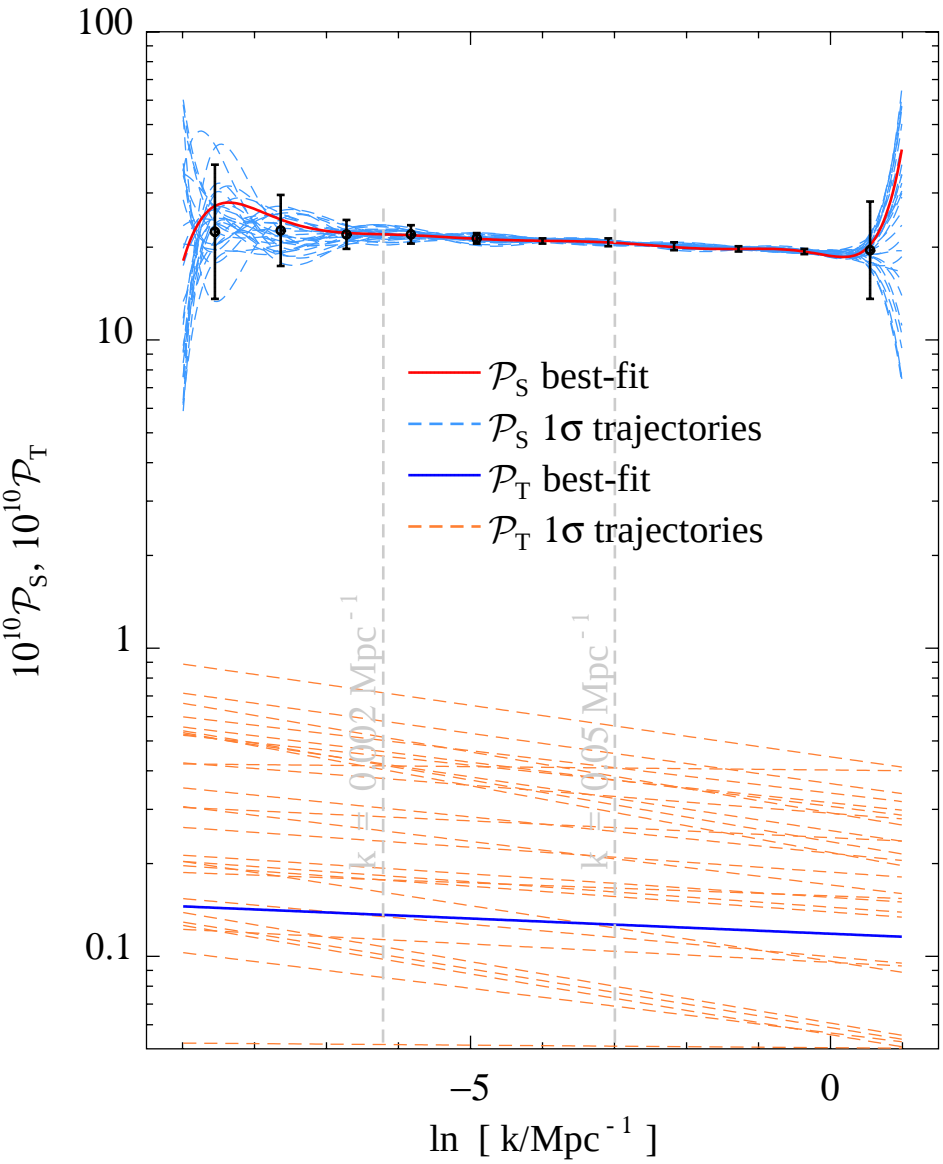

Figure 9. Increasing the number of knots for $\mathcal{P}_s$ leads to oscillations. Mock data with fiducial $r = 0$ has been used.

trajectory, the error bars grow tremendously and the central value shifts considerably.

6.2.4 Model selection

Recently a lot of attention has been devoted to the question of model selection [76, 77]. Given several competing models with different numbers of parameters, the fundamental issue is to decide which model describes the data best while at the same time not introducing "superfluous" parameters whose presence is not warranted by the data. The decision on the usefulness of a parameter is in part based on the volume of parameter space that one subjectively deems likely to be allowed. In this work our approach will be to examine the space of possible inflationary trajectories without introducing any subjective model selection.

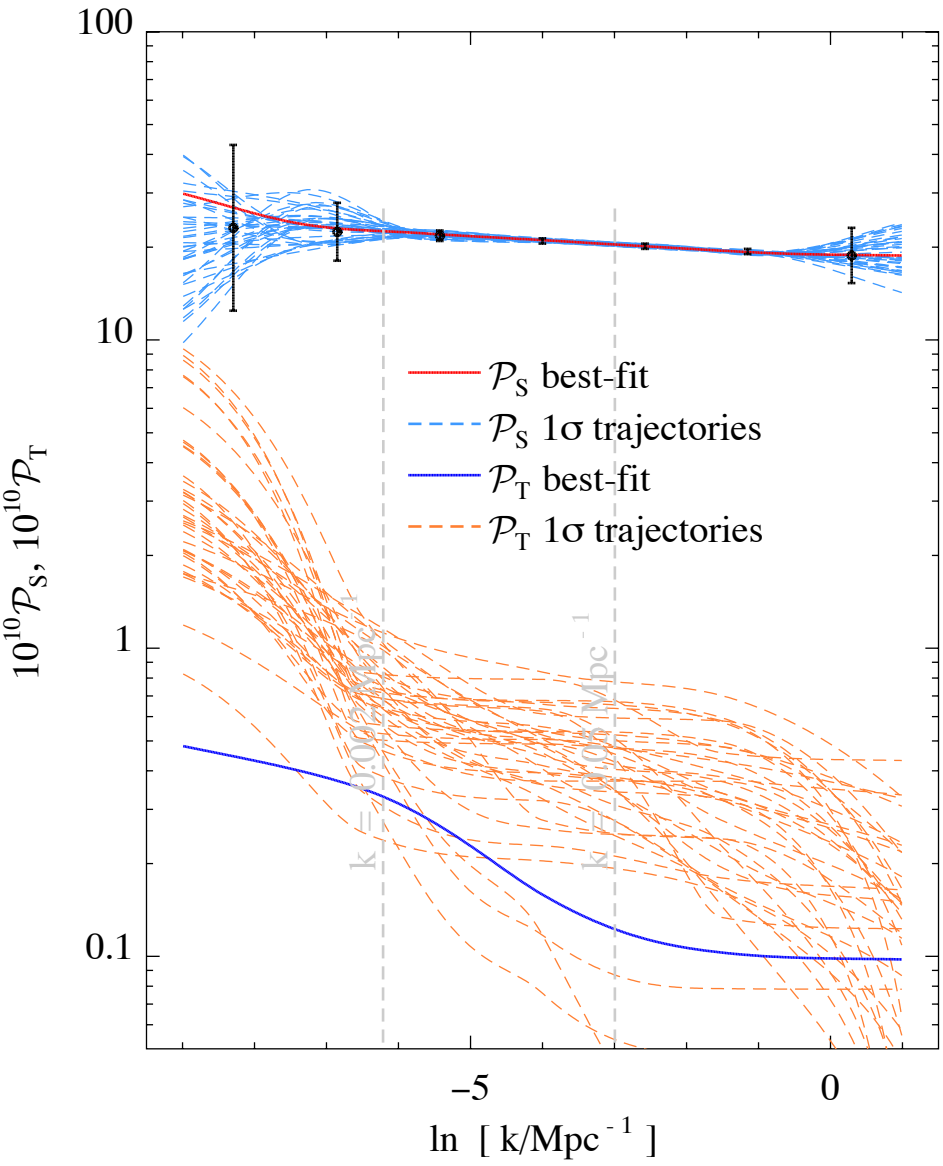

Figure 10. Increasing the number of knots for the tensor power spectrum from 2 degrees of freedom to 5 degrees of freedom, with the monotocity condition $d\ln\mathcal{P}_t/d\ln k < 0$ applied. Mock data with fiducial $r = 0$ have been used here. The uncertainty in the tensor spectrum is driven by the priors.

Our focus will be on the effect the increase in the number of parameters will have on the posterior distribution of the parameters and the implied priors.

6.3 Searching for nontrivial features in the power spectra

Although any specific choice of algorithm to generate "random" trajectories may be challenged by prior issues as discussed above, we are interested in methods that can practically detect nontrivial features in the primordial power spectra. To show that the method we are advocating in this paper is a viable candidate, we produce mock data with $\mathcal{P}_s$ having an

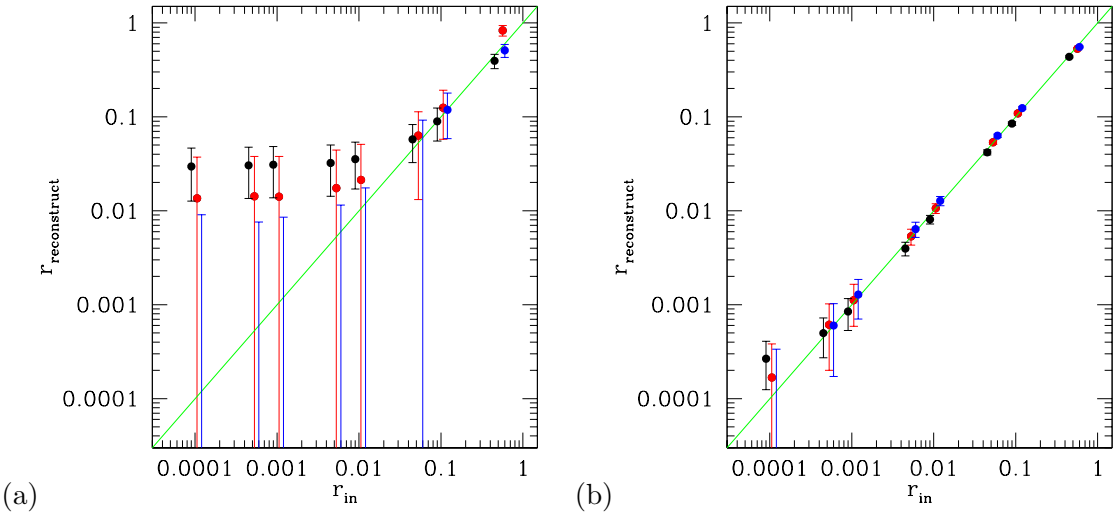

Figure 11. The reconstructed values $r_{\rm reconstructed}$ of the input tensor scalar ratio $r_{\rm in}$ from a (a) Planck and (b) CMBPol type experiment with different parameterizations: $\mathcal{P}_s, \mathcal{P}_t$ (black), the standard parameterization (red), $\ln\epsilon$ trajectories (blue). For a Planck type experiment, the reconstructed values of r are prior dominated at $r \approx 0.05$.

"IR-cascading" bump [15, 16], approximated by

$$P_{\rm bump} = A\left(\frac{k}{k^*}\right)^3 e^{-\frac{\pi}{2}(k/k^*)^2} \ . \tag{6.3}$$

The shape of such a bump can be calculated in the theory, and should be parameterized accordingly in power spectrum reconstruction attempts if we consider this particular model. Here we examine whether such a bump is detectable without knowing the theoretical priori.

The reconstructed power spectra using monotonic cubic Hermite interpolation between 11 knots are shown in Figure 12. The bump in the scalar spectrum has no effect on the reconstructed tensor spectra, we hence only show scalar trajectories in the plot for a clear view of the details of the reconstructed bump. We notice that the bump is successfully reconstructed. However, the spectrum close to the bump is slightly twisted by the smoothness assumption (prior) we have chosen. We have also tried natural cubic spline interpolation and varying the number of the knots. We find that the twisting varies with different choices of interpolation method and number of knots, confirming our conjecture that it is a prior-driven effect. Despite these prior issues that persist in any trajectory reconstruction methods, we are able to find the main feature in the power spectrum without knowing the theoretical priori.

7 Single field inflation models

In this section, we restrict the space of allowed inflationary possibilities to models driven by single real scalar fields. In this case, it is straightforward to see that all information about the inflationary history is encapsulated in the time evolution of the "slow roll" parameter ϵ which we will briefly demonstrate below.

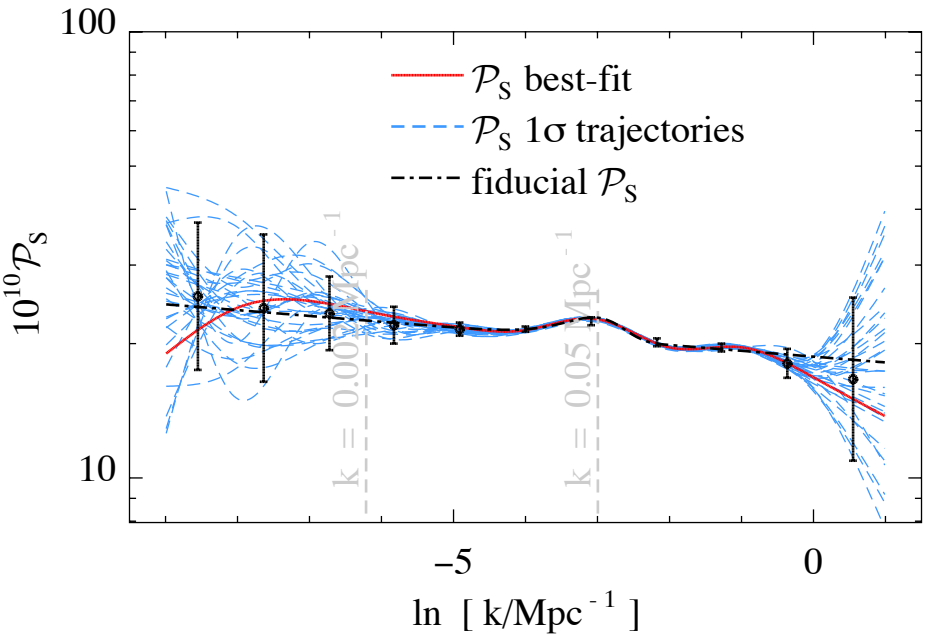

Figure 12. The reconstructed primordial power spectra, using mock data with a feature in the scalar power spectrum. A fiducial $r = 0$ and $n_s = 0.97$ model has been used, on top of which an IR-cascading bump [15, 16] with amplitude about 10% of the total $\mathcal{P}_s$ and with position $k^* = 0.05\,\mathrm{Mpc}^{-1}$ is added to the scalar power spectrum, as shown in dot-dashed black color. Monotonic cubic Hermite interpolation is used to interpolate $\ln \mathcal{P}_s$ between 11 knots.

7.1 Inflation driven by a single scalar field

A brief recap of the physics of inflation driven by a single real scalar field is in order. Assuming the background is given by an FRW metric

$$ds^2 = dt^2 - a(t)^2 d\mathbf{x}^2\,, \tag{7.1}$$

with scale factor a, and permeated by a homogeneous scalar field ϕ obeying

$$\ddot{\phi} + 3H\dot{\phi} + \partial_\phi V = 0\,, \tag{7.2}$$

$$\frac{1}{3}\left(\frac{1}{2}\dot{\phi}^2 + V\right) = H^2\,, \tag{7.3}$$

$$\frac{1}{2}\dot{\phi}^2 = -\dot{H}\,, \tag{7.4}$$

where we introduced the Hubble parameter $H = \partial_t \ln a$ and set the reduced Planck mass to unity $M_p^2 \equiv \frac{1}{8\pi G} = 1$.

It is well known that small perturbations on top of this homogeneous background obey

$$u_k'' + \left(k^2 - \frac{z''}{z}\right) u_k = 0\,, \tag{7.5}$$

$$v_k'' + \left(k^2 - \frac{a''}{a}\right) v_k = 0\,, \tag{7.6}$$

$$\tag{7.7}$$

where u_k, v_k are the perturbations in the scalar and tensor sector and given by

$$u_k = -\frac{a\dot{\phi}}{H}\left(\Psi - \frac{H}{\dot{\phi}}\delta\phi\right), \tag{7.8}$$

$$h_{ij} = \int \frac{d^3k}{(2\pi)^{3/2}} \sum_{\lambda=1}^{2} \frac{1}{a} v_{k,\lambda} e_{ij}(k,\lambda) e^{ikx}, \tag{7.9}$$

where Ψ, h_{ij} is the scalar/ tensor part of the metric perturbation, e_{ij} is the polarization tensor, $z = \sqrt{2\epsilon}a$, and $f' = a\frac{\partial}{\partial t}f$, see [78] for details.

7.2 All information is in ϵ

As mentioned above, all information about the evolution of the universe, i.e. of the background fields and their perturbations, is contained in the time evolution of $\epsilon \equiv -\frac{\dot{H}}{H^2}$. This can be seen by rearranging the background equations (7.2)

$$a = e^{-N}, \tag{7.10}$$

$$\frac{\partial\phi}{\partial N} = \pm\sqrt{2\epsilon}, \tag{7.11}$$

$$\frac{\partial \ln H}{\partial N} = -\epsilon, \tag{7.12}$$

$$V = H^2(3-\epsilon), \tag{7.13}$$

where $dN = -Hdt$ is the number of e-folds, so that there is a mapping from a given expansion history $\epsilon(t)$ plus an integration constant for H to a scalar field potential that allows for such a ϵ trajectory. Note that the integration constant for ϕ is irrelevant as this corresponds to a constant shift of the potential, whereas the sign ambiguity is due to the fact that sending $\phi \to -\phi$ does not change the physics either.

Most importantly, for a given energy scale $H(k_{\rm pivot})$, $\epsilon(t)$ is all that is needed to plug into the perturbation equations (7.5), so that knowledge of ϵ also completely determines the knowledge of the perturbation spectra.

It should also be noted that instead of providing ϵ as a function of some time variable, it is equally viable to provide it as a function of the (comoving) wavenumber k, making use of the fact that inflationary perturbations of wavenumber k freeze out around the time when $k \lesssim aH$ (although see [79] for an inflationary model in which perturbations do not freeze out).

In short, having full knowledge of $\epsilon(k) \equiv \epsilon|_{k=\ln(aH)}$ trajectories, it is straightforward to compute the scalar potential as well as the behavior of the scalar and vector perturbations.

7.3 The ϵ trajectory and different priors

Working with ϵ as a trajectory has another advantage: it is well known that the inflationary condition $\ddot{a} > 0$ is equivalent to

$$\ddot{a} \equiv a(\dot{H} + H^2) = aH^2(1-\epsilon) \overset{!}{>} 0\,. \tag{7.14}$$

In other words, $\epsilon < 1$ during a period of accelerated expansion. On the other hand, for an expanding universe $\epsilon \equiv -\frac{\dot{H}}{H^2} > 0$ as $\dot{H} < 0$. Thus, ϵ trajectories during inflation are required to lie between

$$0 < \epsilon < 1\,. \tag{7.15}$$

It should be noted that this "inflationary prior" is not realized by the usual approach to model building. Writing down models for single field inflation usually means writing down a potential for ϕ (possibly as a power series). This does not give a uniform prior for ϵ between $[0, 1]$, but rather a strong preference for "slow roll" models, that is, models with $\epsilon \ll 1$ and $|d\ln\epsilon/d\ln k| \ll 1$. While this is a valid subjective choice of prior, it seems an interesting questions as to what the data prefers if we do not employ this slow roll prior. In particular, the condition $|d\ln\epsilon/d\ln k| \ll 1$ can be relaxed to some extent without spoiling a nearly scale invariant scalar power spectrum.

Unfortunately, it turns out that using straight $\epsilon(\ln k)$ trajectory functions introduces spurious detections of tensors which are purely prior driven: even though the values of the trajectory function at the knots are chosen uniformly between $[0, 1]$, the interpolation leads to a systematic bias against small values of ϵ, see Appendix B. Hence we need to slightly change the trajectory function.

Most interest lies in the spectra index $n_s - 1 \approx -2\epsilon - d\ln\epsilon/d\ln k$ (which is also well constrained by data). In the case that ϵ is small, the deviation from scale-invariance of the scalar power spectrum is due to the term $\frac{d\ln\epsilon}{d\ln k}$. This makes it a suitable choice of trajectory function. However, it slightly complicates the step of verifying that the trajectory corresponds to an inflating universe, but avoids the purely prior driven detection of tensors.

Figure 13 shows the reconstructed power spectra when using a 7 knot cubic Hermite polynomial expansion of $\frac{d\epsilon}{d\ln k}$. The best-fit trajectories are shown in solid red, whereas the trajectories from the 1σ interval are plotted in solid blue. Even though there are some features in $\mathcal{P}_S$ (Figure 13a), the corresponding C_ℓ^{TT} spectra (Figure 13b) agree very well with observations.

As can be seen in Figure 14(a), the underlying ϵ trajectories are relatively smooth within the interval $\ln\frac{k}{\mathrm{Mpc}^{-1}} = -5\ldots0$. On larger scales, there are some wild excursions with ϵ even becoming non-monotonic. Yet the overall smoothness of the ϵ trajectory is quite striking, given the fact that the extrapolation used 7 knots – a relatively large number. For comparison, the unconstrained $\mathcal{P}_s, \mathcal{P}_t$ expansion of the previous section contained much wilder trajectories when using 7 knots for $\mathcal{P}_s$.

7.4 Reconstructing the potential

As mentioned above, all information about single field inflation is contained in the ϵ trajectory. In particular, we can reconstruct the shape of the scalar field potential $V(\phi)$ from knowledge of the (time) evolution of ϵ.

This is most readily achieved by rewriting Eq. (7.10) as

$$V(\ln k) = H^2(\ln k)\,(3 - \epsilon(\ln k))\,, \tag{7.16}$$

$$\frac{\partial\phi}{\partial\ln k} = \pm\frac{\sqrt{2\epsilon(\ln k)}}{1-\epsilon(\ln k)}\,, \tag{7.17}$$

$$\frac{\partial\ln H}{\partial\ln k} = -\frac{\epsilon(\ln k)}{1-\epsilon(\ln k)}\,. \tag{7.18}$$

This allows us to map the reconstructed ϵ trajectories from Figure 14(a) to the potential $V(\phi)$, see Figure 14(b). The red line represents the best fit potential, whereas the blue lines are drawn from the 1σ interval around the best fit. Note that both the potential has been rescaled and the field values shifted so that the differences in shape become more apparent.

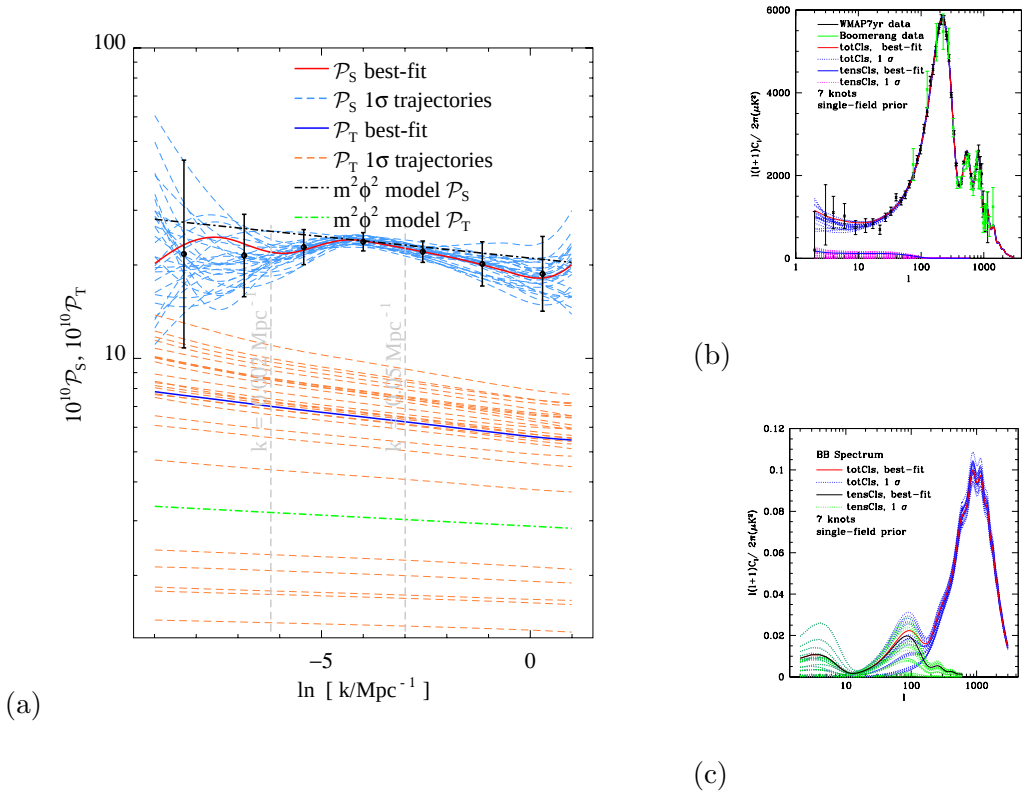

Figure 13. (a)Reconstructed power spectra when using a 7 knots expansion of the $\frac{d\epsilon}{d\ln k}$ trajectory. (b) TT angular power spectrum (c) BB angular power spectrum. Same color scheme as in Figures 3, 5

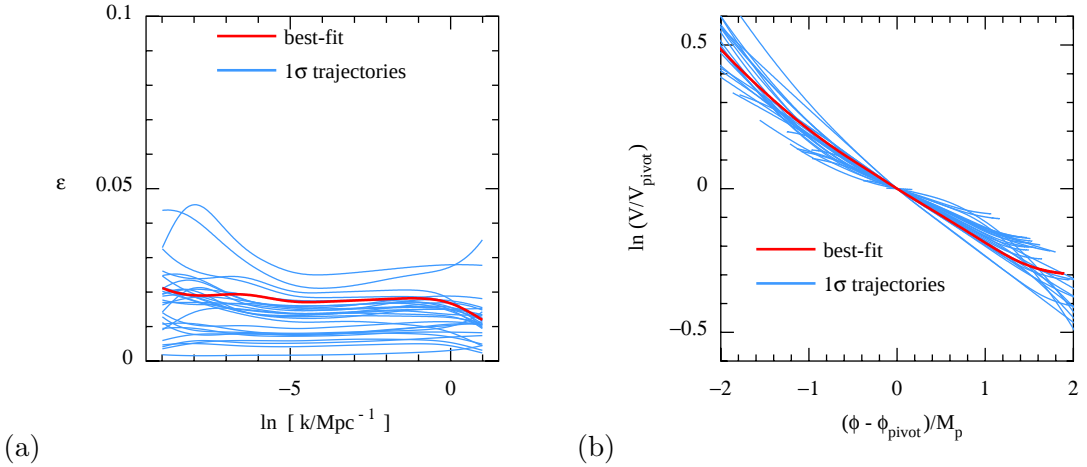

Figure 14. (a) ϵ trajectory using an order 7 knots, natural monotonic cubic Hermite interpolation of the ϵ trajectory and (b) Reconstructed potentials. The best fit trajectories are shown in red, and the ones drawn from the 1σ interval around it in blue.

Just as with the independent tensor and scalar spectra about, we shall now briefly discuss the performance of using ϵ trajectories with forecast data. We examine the same two

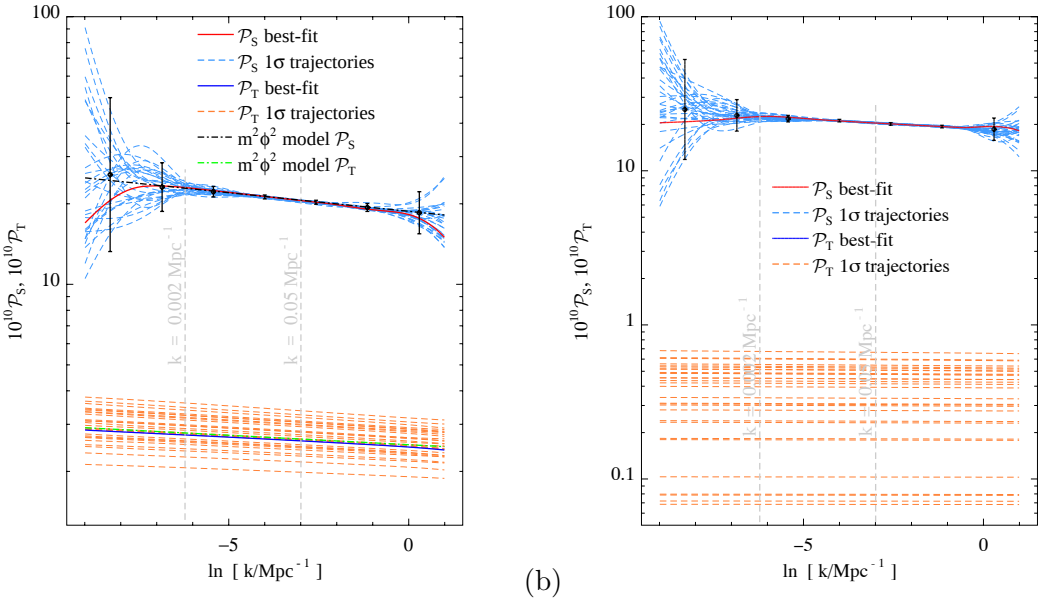

Figure 15. (a) Forecast for $m^2\phi^2$ inflation with $r = 0.13$, $n_s = 0.97$ (b) Forecast for single field inflation with $r = 0$.

fiducial models as in Section 6.1.

For the fiducial $V(\phi) = m^2\phi^2$ model with $r = 0.13$, Figure 15 shows that using the ϵ trajectories, both the scalars and tensors are reconstructed with high precision. The reason for this improvement in performance over the independent $\mathcal{P}_s$, $\mathcal{P}_t$ trajectories is the additional theoretical information we added to the picture: the fact that scalars and tensors obey the consistency condition $n_t = -\frac{r}{8}$. In this framework, a well constrained scalar spectrum will automatically induce small error bars on the tensors.

8 Summary and Conclusions

In this paper we study different ways to scan over inflationary models in order to explore the range of primordial power spectra that can be generated. We investigate the inverse problem of how to reconstruct the primordial power spectra of scalar and tensor perturbations from observational data.

While most of the previous studies on the ensemble of inflationary models used a diversity of potential functions $V(\phi)$, we focus instead on the trajectory functions, as described by the evolution of $\mathcal{P}_s$, $\mathcal{P}_t$ or ϵ during inflation.

If the time flow along of the inflationary trajectory is measured in terms of number of e-foldings N, the minimum duration of inflation ΔN generally depends on the inflationary model. The time interval during which the inflationary trajectories are examined can be made precisely independent of the model if time is measured in comoving momenta of fluctuations $\ln k$ provided one assumes that inflation does not proceed in staggered phases. Thus we are dealing with an ensemble of trajectory functions over a fixed domain of the argument which can be conveniently expanded in various function bases such as Chebyshev polynomials or B-splines, providing both optimal approximation and numerically fast routines for evaluation and taking derivatives.

We demonstrate explicitly how the traditional parameterization using $A_s, n_s, n_{\rm run}, r$ is exactly equivalent to a specific trajectory approach and show that the parameters reconstructed by both parameterizations are in very good agreement. As a further test of reliability, we show that simulated spectra smeared by Planck errors can be reconstructed with $\mathcal{P}_s, \mathcal{P}_t$ as well as ϵ trajectories – albeit with some residual uncertainty pertaining to the shape of the (implicit) prior distributions.

In contrast to existing methods like the flow equations, the scanning inflation approach as presented here does not involve any integration of differential equations, making it numerically extremely fast. The trajectory choice of $\mathcal{P}_s, \mathcal{P}_t$ does not respect the consistency relation connecting them in the case of inflation driven by a scalar field. Of particular importance, we have shown that nontrivial features in the scalar power spectrum can be detected without using theoretical prior knowledge about the shape of the feature.

Incorporating the consistency relation naturally leads to taking another choice for the trajectory function, the deceleration parameter ϵ, where it becomes necessary to perform a single integration to obtain the Hubble trajectory needed to compute the power spectra. In this case, one can describe all inflationary dynamics (both of the background and the perturbations) in terms of the evolution of e.g. $\epsilon(\ln k)$, also reconstructing the shape of the potential of the scalar field driving inflation.

We identified the importance of priors and the ways their bias can change the outcome of MCMC parameter estimation. Even though parameters are sampled with flat priors, the prior distribution of the power spectra can be implicitly altered, a fact that is easy to overlook. Exploring various choices of priors, we demonstrated that it is possible to at least partially smooth the inhomogeneity of the priors, making the distribution uniform and only slightly depending on the position in k-space.

Implied priors most significantly impact the value of the tensor scalar ratio r. Using a uniform and homogeneous prior on $\ln \mathcal{P}_s, \mathcal{P}_t$ in an expansion to order $(3, 1)$ – i.e. a constant tensor spectrum –, the upper limit on $r < 0.33(95\%\text{CL})$ is compatible with the limit $r < 0.36(95\%\text{CL})$ obtained using the standard parameterization given the fact that the parameters trajectory parameterization are non-linear combinations of the standard parameters.

Let us finish with a final remark on the maximum amount of complexity that can be present in inflationary trajectories. In principle, one can increase the expansion order to arbitrarily high numbers, allowing for more and more structure in the trajectories. Here we conjecture[3] that there is a natural limitation on the structure and fine details of the trajectories, namely that the details associated with features on time scales smaller than the inverse Hubble scale H^{-1} are irrelevant. This is to say only those features on a scale exceeding one e-folding are relevant. There are numerous examples in the literature with the calculations of the spectra from inflation with various features like breaks in the potentials, marginal inflation etc. All of them show that the features of the corresponding power spectra are smooth on scales less than H. Heuristically it can be understood by analogy with diffraction patterns in wave optics, where in our case the wavelength of interest is H^{-1}.

This conjecture implies that in order to exhaust all potential inflationary trajectories describing the physics in the k-range accessible to observations – i.e. about 10 e-folds – it is sufficient to consider trajectories only up to order 10, making inflation a science of only 10 numbers.

[3]We thank Andrei Linde for useful discussions of this point.

Acknowledgments

All computations were performed on thecomputing clusters at CITA. We gratefully acknowledge financial support by NSERC, CIFAR and CFI.

A Various function bases

The current observational data explore about ten e-folds of comoving wave-length, roughly corresponding to the interval $-9 < \ln\left(k/\mathrm{Mpc}^{-1}\right) < 1$. Let us define this interval as "observable interval". The spectra on scales outside the observable interval do not have essential impact on the cosmic observables. Any reasonable extrapolation will do as good. We simply use constant $\mathcal{P}_s$ for these extra-large and extra-small scales. Natural cubic spline interpolation is our default option to interpolate $\ln \mathcal{P}_s$ within the observable interval. Alternative interpolation methods are Chebyshev interpolation and monotonic cubic Hermite interpolation. The Chebyshev interpolation defines a unique $n-1$-th order polynomial passing the n given points at the knots. Both natural cubic spline interpolation and monotonic cubic Hermite interpolation assume third order polynomial between two neighbor knots. Natural cubic spline defines a unique interpolated curve by matching the second order derivatives across the knots, with an additional assumption that the second order derivative vanishes at the two boundaries. The cubic Hermite interpolation only requires the first order derivative to be continuous across the knots. The extra n degrees of freedom is fixed by choosing the first order derivative at the i-th knot. For generic cubic Hermite interpolation where the piecewise monotonicity is not required, the derivatives can be chosen as

$$\Delta_i \equiv \begin{cases} \left[f(x_2)-f(x_1)\right]/(x_2-x_1) & \text{, if } i=1 \\ \left[f(x_n)-f(x_{n-1})\right]/(x_n-x_{n-1}) & \text{, if } i=n \\ \left[f(x_{i+1})-f(x_{i-1})\right]/(x_{i+1}-x_{i-1}) & \text{, else} \end{cases} \tag{A.1}$$

where x_i is the i-th knot. For monotonic cubic Hermite interpolation, the piecewise monotonicity of $f(x)$ between two neighbor knots is achieved by further adjusting Δ_i. First, for $i = 1, 2, ..., n-1$, if $f(x_i) = f(x_{i+1})$, set $\Delta_i = \Delta_{i+1} = 0$. Second, for $i = 1, 2, ..., n-1$ where $f(x_i) \neq f(x_{i+1})$, define $\alpha_i = \Delta_i(x_{i+1}-x_i)/\left[f(x_{i+1})-f(x_i)\right]$ and $\beta_i = \Delta_{i+1}(x_{i+1}-x_i)/\left[f(x_{i+1})-f(x_i)\right]$; If $\alpha_i^2+\beta_i^2 > 9$, update Δ_i and Δ_{i+1} to be $3\alpha_i\Delta_i/\sqrt{\alpha_i^2+\beta_i^2}$ and $3\beta_i\Delta_{i+1}/\sqrt{\alpha_i^2+\beta_i^2}$, respectively.

To summarize, the parameterization is:

1. Flat prior on $\ln \mathcal{P}_s$, if k is a knot.
2. Interpolate $\ln \mathcal{P}_s(\ln k)$, if $-9 < \ln\left(k/\mathrm{Mpc}^{-1}\right) < 1$ and k is not a knot.
3. Extrapolation: $\ln \mathcal{P}_s(\ln k) = \ln \mathcal{P}_s\,|_{\ln\left(k/\mathrm{Mpc}^{-1}\right)=-9}$, if $\ln\left(k/\mathrm{Mpc}^{-1}\right) < -9$; $\ln \mathcal{P}_s(\ln k) = \ln \mathcal{P}_s\,|_{\ln\left(k/\mathrm{Mpc}^{-1}\right)=1}$, if $\ln\left(k/\mathrm{Mpc}^{-1}\right) > 1$.

Uniformly distributed knots from $\ln(k/\mathrm{Mpc}^{-1}) = -9$ to $\ln(k/\mathrm{Mpc}^{-1}) = 1$ are used for natural cubic spline interpolation and monotonic cubic Hermite interpolation. For Chebyshev interpolation we choose the nodal points of Chebyshev polynomials, i.e., the n solutions of n-th order Chebyshev polynomial $T_n(x) = 0$, with $x \equiv \frac{\ln(k/\mathrm{Mpc}^{-1})+4}{5}$. The Chebyshev polynomials along with the particular pattern of knots are used for better fitting and numerical stability [80].

B Implicit Priors of Random Trajectories

In this appendix we examine the priors that are implicit in the choice of trajectory function and their impact on parameter estimation via Markov Chain Monte Carlo (MCMC) algorithms in detail.

Traditionally assuming inflation driven by a scalar field, the prior for inflationary models is that $V(\phi)$ is sufficiently flat and smooth such that the primordial power spectra are only mildly broken scale invariant and can be parameterized by $(n_s, n_{\rm run}, r)$. Ignoring this theoretical bias, the interpolating functions in the scanning approach will allow for radically broken scale invariance. Using different trajectory functions and expansion bases, we shall investigate the shape of the implied priors on the traditional parameters.

We generate an ensemble of spectral trajectories $\mathcal{P}_t$ using the methods based on the Chebyshev decomposition described in Section 6 and demonstrate how the positivity requirement for $\mathcal{P}_t$ influences the prior.

The function $\mathcal{P}_t$ must be positive $\mathcal{P}_t > 0$ with a negative slope $\frac{d\mathcal{P}_t}{d\ln k} < 0$ because Hubble is a decreasing function of time. This implies that even though the values of $\mathcal{P}_t$ at the nodal points are sampled with a uniform prior, the prior distribution of $\mathcal{P}_t$ on and especially in between nodal points is rather complex and peaked at a value larger than zero, see Figure 16. Panel (a) of this figure shows the prior probability distribution of a non monotonic Chebyshev interpolation of $\mathcal{P}_t$ to order 5 at the third nodal point (black solid curve) and in between nodal points (red dashed curve). At the nodal point, the distribution should ideally be flat, however due to the positivity of $\mathcal{P}_t$ the probability distribution falls off towards lower values of $\mathcal{P}_t$. In between nodal points, an interpolation effect is responsible for the peak of the probability distribution:

Naively one might expect that sampling uniformly a trajectory function at a number of nodal points in $\ln k$ and interpolating would also lead to a more or less uniform distribution of function values in between the sampled points. But this is only true for functions which do not have to fulfill any constraints. In case there are any restrictions on the functions, e.g. enforcing positivity of $\mathcal{P}_s, \mathcal{P}_t$, or restricting them to a finite range, the prior will generally depend on the location in k-space, changing the picture dramatically. In case of constrained trajectory functions, the prior distribution becomes peaked away from zero despite being flat at nodal points. This can be understood in terms of a simple frequentist argument for example in a linear interpolation between two points $(A, y(A)), (B, y(B))$, denoted by the red dots in Figure 17a. The vertical position of both points is chosen with a uniform prior $P(A) = P(B) = 1$, $(y(A), y(B)) \in [0, 1]$. For the value of $y(C)$ to be zero, both $y(A)$ and $y(B)$ have to be zero, whereas for say $y(C) = 0.5$, the pair $(y(A), y(B))$ can have values $(1.0, 0.0), (0.999, 0.001), \ldots$, therefore it is much more likely for $y(C)$ to be 0.5 than to be zero.

Performing a more quantitative analysis of the situation, it is straightforward to calculate the prior distribution of the point $y(C)$ which is located in the midpoint between A and B,

$$\begin{aligned} P(C) &= \int_0^1 dA \int_0^1 dB\, P(A)P(B) \\ &\qquad \times \delta\left(C - (A + (B - A)/2)\right) \\ &= \begin{cases} 4(1-C), & \frac{1}{2} < C \leq 1 \\ 4C, & 0 \leq C \leq \frac{1}{2} \end{cases}, \end{aligned} \tag{B.1}$$

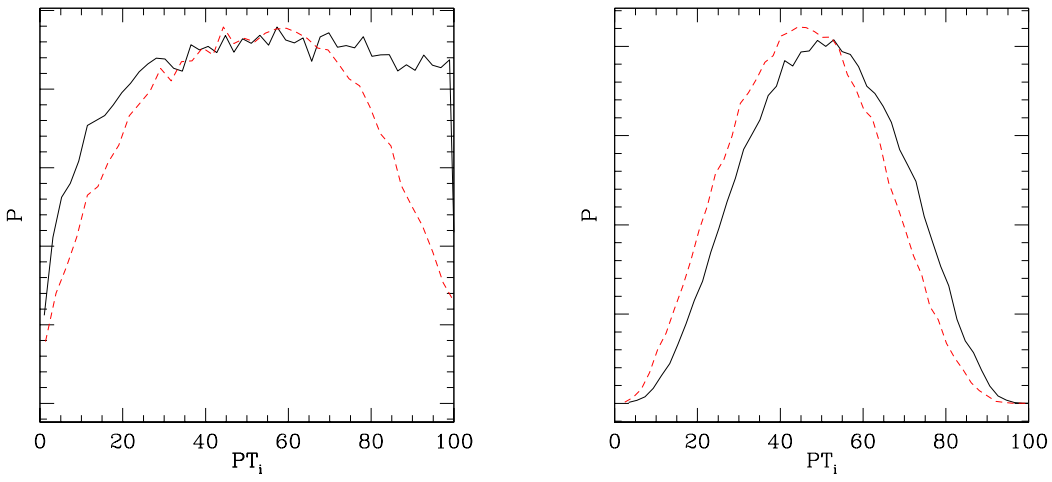

(a) (b)

Figure 16. The prior probability distribution of a Chebyshev interpolation of $\mathcal{P}_t$ to order 5 at the third nodal point (black solid curves) and in between nodal points (red dashed curves) for (a)non monotonic and (b) monotonic $\mathcal{P}_t$. The fall-off of the distribution at lower values of $\mathcal{P}_t$ even on the nodal point is due to the fact that non-physical trajectories, i.e. those with $\mathcal{P}_t < 0$, are rejected. Therefore if the values at the third nodal point is close to zero, trajectories can potentially dip below zero and therefore will be discarded. In between nodal points, interpolation effects cause the distribution to be peaked. In the monotonic case, even at the nodal points enforcing monotonicity makes the distribution fall off at high values of $\mathcal{P}_t$, so that the distribution is peaked even at the nodal points, and the only effect of moving away from the nodal points is a slight shift in the position of the peak.

to be shaped like a triangle, see Figure 17(b). Using any expansion basis for interpolation, the prior distribution of the spectral trajectories in between nodal points therefore is not uniform either.

This effect can significantly alter the outcome of MCMC parameter reconstruction runs as we will see below. Most prominently it can lead to a spurious "detection" of tensors using the Chebyshev procedure as all trajectory functions $\mathcal{P}_t$ related to the tensor scalar ratio r are constrained to be positive.

Using B-splines as basis functions, we also find that the priors are also heavily dependent on the order of the expansion and on the choice of trajectory, i.e. whether we use n_t or $\mathcal{P}_t$ as spectral trajectory. Figure 18 shows the prior distribution of the tensor amplitude $\mathcal{P}_t$ at $k = 0.002\text{Mpc}^{-1}$ for an 8 parameter third order B-spline expansion. It is immediately obvious that the apparent detection of tensors (solid line) is solely caused by the prior (dashed line) implied in this expansion. Generating spectral trajectories $\mathcal{P}_t$ without requiring monotonicity, the prior shows a moderate favor for medium values, caused by the interpolation effect mentioned above. The asymmetry stems from the fact that the point $k = 0.002\text{Mpc}^{-1}$ is not exactly in the middle between two nodal points.

Enforcing monotonicity of $\mathcal{P}_t$, the prior shows a strong favor of large values (panel (a)).

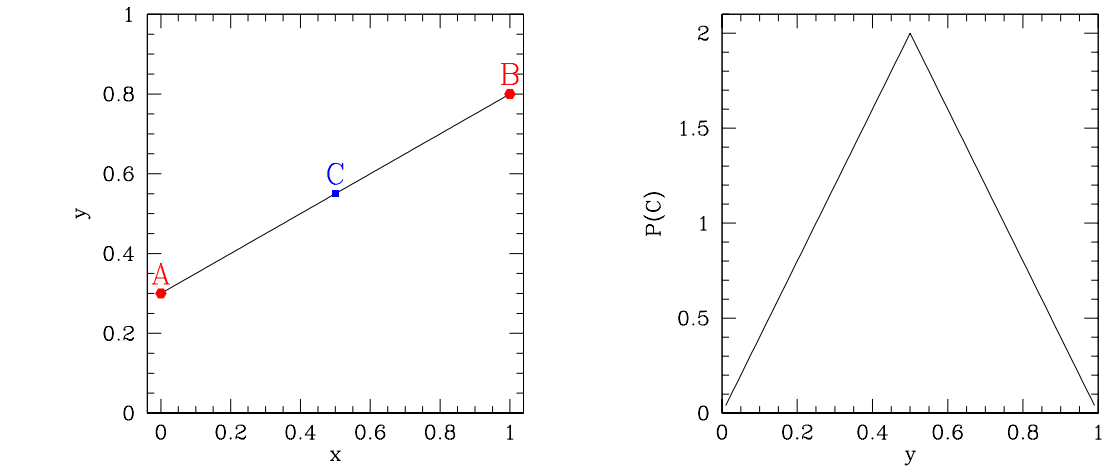

(a) (b)

Figure 17. (a) Linear interpolation between two points A, B. A, B are drawn from $[0, 1]$ with uniform prior (b) The probability distribution of point C, located in the middle between A and B.

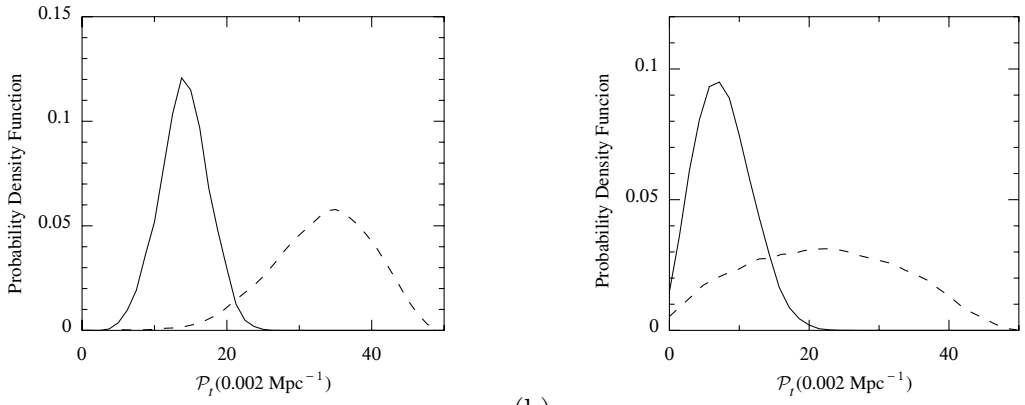

(a) (b)

Figure 18. Prior (dashed) and posterior (solid) distribution of the tensor power $\mathcal{P}_t$ at $k = 0.002\mathrm{Mpc}^{-1}$ for an eight parameter B-spline expansion. The apparent detection of r in the posterior is clearly an effect of the implicit prior. (a) monotonic $\mathcal{P}_t$. (b) non-monotonic $\mathcal{P}_t$.

Two effects are responsible for this: the interpolation effect as elaborated above, and the fact that monotonicity makes the prior position dependent even at nodal points, see Figure 19. If $\mathcal{P}_t$ is monotonically decreasing with k, the values at smaller k must be larger on average than the values at larger k. Going towards medium values of $\ln k$, the distribution becomes uniform, and finally at large values of $\ln k$, small values of $\mathcal{P}_t$ are strongly favored. The point $k = 0.002\mathrm{Mpc}^{-1}$ lies in the left half of k-space, therefore the prior favors larger values of the tensor amplitude.

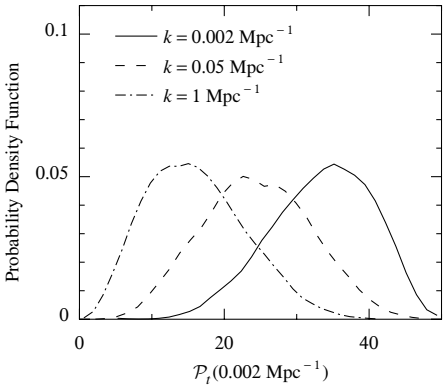

Figure 19. Prior distribution of a monotonically decreasing trajectory $\mathcal{P}_t$. Going from small values of $\ln k$ (solid) over intermediate (dashed) to large values of $\ln k$ (dashed-dotted), the distribution's shape changes significantly.

The bottom line is that different parameterizations imply different priors. When thinking about parameterizing the primordial spectra (or any other quantity that is not well constrained by current observational data), great care must be taken to accurately take into account the effects of the priors.

References

[1] D. J. Fixsen et al. The cosmic microwave background spectrum from the full cobe/firas data set. *Astrophys. J.*, 473:576, 1996, astro-ph/9605054.

[2] C. B. Netterfield et al. A measurement by BOOMERANG of multiple peaks in the angular power spectrum of the cosmic microwave background. *Astrophys. J.*, 571:604–614, 2002, astro-ph/0104460.

[3] D. N. Spergel et al. First year wilkinson microwave anisotropy probe (wmap) observations: Determination of cosmological parameters. *Astrophys. J. Suppl.*, 148:175, 2003, astro-ph/0302209.

[4] G. Hinshaw et al. Three-year wilkinson microwave anisotropy probe (wmap) observations: Temperature analysis. 0300, astro-ph/0603451.

[5] E. Komatsu et al. Five-Year Wilkinson Microwave Anisotropy Probe (WMAP) Observations:Cosmological Interpretation. 2008, 0803.0547.

[6] E. Komatsu et al. Seven-Year Wilkinson Microwave Anisotropy Probe (WMAP) Observations: Cosmological Interpretation. 2010, 1001.4538.

[7] Planck: The scientific programme. 2006, astro-ph/0604069.

[8] Shamit Kachru, Renata Kallosh, Andrei Linde, and Sandip P. Trivedi. De sitter vacua in string theory. *Phys. Rev.*, D68:046005, 2003, hep-th/0301240.

[9] J. J. Blanco-Pillado, C. P. Burgess, J. M. Cline, C. Escoda, M. Gomez-Reino, R. Kallosh, A. Linde, and F. Quevedo. Racetrack inflation. *JHEP*, 11:063, 2004, hep-th/0406230.

[10] J. J. Blanco-Pillado, C. P. Burgess, J. M. Cline, C. Escoda, M. Gomez-Reino, R. Kallosh, A. Linde, and F. Quevedo. Inflating in a better racetrack. *JHEP*, 09:002, 2006, hep-th/0603129.

[11] S. Kachru, R. Kallosh, A. Linde, J. Maldacena, L. McAllister, and S. P. Trivedi. Towards inflation in string theory. *JCAP*, 0310:013, 2003, hep-th/0308055.

[12] Joseph P. Conlon and Fernando Quevedo. Kaehler moduli inflation. *JHEP*, 01:146, 2006, hep-th/0509012.

[13] Steven B. Giddings, Shamit Kachru, and Joseph Polchinski. Hierarchies from fluxes in string compactifications. *Phys. Rev.*, D66:106006, 2002, hep-th/0105097.

[14] Eva Silverstein and Alexander Westphal. Monodromy in the CMB: Gravity Waves and String Inflation. *Phys. Rev.*, D78:106003, 2008, 0803.3085.

[15] N. Barnaby, Z. Huang, L. Kofman, and D. Pogosyan. Cosmological fluctuations from infrared cascading during inflation. Phys. Rev. D, 80(4):043501–+, August 2009, 0902.0615.

[16] Neil Barnaby and Zhiqi Huang. Particle production during inflation: Observational constraints and signatures. *Phys. Rev. D*, 80(12):126018, Dec 2009.

[17] J. R. Bond, A. V. Frolov, Z. Huang, and L. Kofman. Non-Gaussian Curvature Spikes from Chaotic Billiards in Inflation Preheating. *Physical Review Letters*, 103(7):071301–+, August 2009, 0903.3407.

[18] Andrei D. Linde and Viatcheslav F. Mukhanov. Nongaussian isocurvature perturbations from inflation. *Phys. Rev.*, D56:535–539, 1997, astro-ph/9610219.

[19] David H Lyth and David Wands. The CDM isocurvature perturbation in the curvaton scenario. *Phys. Rev.*, D68:103516, 2003, astro-ph/0306500.

[20] A. A. Starobinsky. Beyond the simplest inflationary cosmological models. *Gravitation and Cosmology*, 4:88–99, 1998, arXiv:astro-ph/9811360.

[21] J. Richard Bond, Lev Kofman, Sergey Prokushkin, and Pascal M. Vaudrevange. Roulette inflation with kaehler moduli and their axions. *Phys. Rev.*, D75:123511, 2007, hep-th/0612197.

[22] Hiranya Peiris and Richard Easther. Slow roll reconstruction: Constraints on inflation from the 3 year wmap dataset. *JCAP*, 0610:017, 2006, astro-ph/0609003.

[23] Hiranya Peiris and Richard Easther. Recovering the inflationary potential and primordial power spectrum with a slow roll prior: Methodology and application to wmap 3 year data. *JCAP*, 0607:002, 2006, astro-ph/0603587.

[24] Antony Lewis and Sarah Bridle. Cosmological parameters from cmb and other data: a monte-carlo approach. *Phys. Rev.*, D66:103511, 2002, astro-ph/0205436.

[25] N. Jarosik et al. Seven-Year Wilkinson Microwave Anisotropy Probe (WMAP) Observations: Sky Maps, Systematic Errors, and Basic Results. 2010, 1001.4744.

[26] The ACT Collaboration, J. W. Fowler, V. Acquaviva, P. A. R. Ade, P. Aguirre, M. Amiri, J. W. Appel, L. F. Barrientos, E. S. Battistelli, J. R. Bond, B. Brown, B. Burger, J. Chervenak, S. Das, M. J. Devlin, S. R. Dicker, W. B. Doriese, J. Dunkley, R. Dünner, T. Essinger-Hileman, R. P. Fisher, A. Hajian, M. Halpern, M. Hasselfield, C. Hernández-Monteagudo, G. C. Hilton, M. Hilton, A. D. Hincks, R. Hlozek, K. M. Huffenberger, D. H. Hughes, J. P. Hughes, L. Infante, K. D. Irwin, R. Jimenez, J. B. Juin, M. Kaul, J. Klein, A. Kosowsky, J. M. Lau, M. Limon, Y. -. Lin, R. H. Lupton, T. A. Marriage, D. Marsden, K. Martocci, P. Mauskopf, F. Menanteau, K. Moodley, H. Moseley, C. B. Netterfield, M. D. Niemack, M. R. Nolta, L. A. Page, L. Parker, B. Partridge, H. Quintana, B. Reid, N. Sehgal, J. Sievers, D. N. Spergel, S. T. Staggs, D. S. Swetz, E. R. Switzer, R. Thornton, H. Trac, C. Tucker, L. Verde, R. Warne, G. Wilson, E. Wollack, and Y. Zhao. The Atacama Cosmology Telescope: A Measurement of the 600 ¡ ell ¡ 8000 Cosmic Microwave Background Power Spectrum at 148 GHz. *ArXiv e-prints*, January 2010, 1001.2934.

[27] H. C. Chiang et al. Measurement of CMB Polarization Power Spectra from Two Years of BICEP Data. *Astrophys. J.*, 711:1123–1140, 2010, 0906.1181.

[28] : P. G. Castro et al. Cosmological Parameters from the QUaD CMB polarization experiment. *Astrophys. J.*, 701:857–864, 2009, 0901.0810.

[29] C. L. Reichardt et al. High resolution CMB power spectrum from the complete ACBAR data set. *Astrophys. J.*, 694:1200–1219, 2009, 0801.1491.

[30] Chao-Lin Kuo et al. Improved Measurements of the CMB Power Spectrum with ACBAR. *Astrophys. J.*, 664:687, 2007, astro-ph/0611198.

[31] M. C. Runyan et al. ACBAR: The Arcminute Cosmology Bolometer Array Receiver. ApJS, 149:265–287, December 2003, arXiv:astro-ph/0303515.

[32] J. H. Goldstein et al. ApJ, 599:773–785, December 2003, arXiv:astro-ph/0212517.

[33] J. L. Sievers et al. Implications of the Cosmic Background Imager Polarization Data. ApJ, 660:976–987, May 2007.

[34] A. C. S. Readhead et al. Extended Mosaic Observations with the Cosmic Background Imager. ApJ, 609:498–512, July 2004, arXiv:astro-ph/0402359.

[35] A. C. S. Readhead et al. Polarization Observations with the Cosmic Background Imager. *Science*, 306:836–844, October 2004, arXiv:astro-ph/0409569.

[36] T. J. Pearson et al. The Anisotropy of the Microwave Background to l = 3500: Mosaic Observations with the Cosmic Background Imager. ApJ, 591:556–574, July 2003, arXiv:astro-ph/0205388.

[37] W. C. Jones et al. Observations of the temperature and polarization anisotropies with BOOMERANG 2003. *New Astronomy Review*, 50:945–950, December 2006.

[38] F. Piacentini et al. A Measurement of the Polarization-Temperature Angular Cross-Power Spectrum of the Cosmic Microwave Background from the 2003 Flight of BOOMERANG. ApJ, 647:833–839, August 2006, arXiv:astro-ph/0507507.

[39] Thomas E. Montroy et al. A Measurement of the CMB Spectrum from the 2003 Flight of BOOMERANG. *Astrophys. J.*, 647:813, 2006, astro-ph/0507514.

[40] Clive Dickinson et al. High sensitivity measurements of the CMB power spectrum with the extended Very Small Array. *Mon. Not. Roy. Astron. Soc.*, 353:732, 2004, astro-ph/0402498.

[41] S. Hanany et al. MAXIMA-1: A Measurement of the Cosmic Microwave Background Anisotropy on angular scales of 10 arcminutes to 5 degrees. *Astrophys. J.*, 545:L5, 2000, astro-ph/0005123.

[42] R. A. Sunyaev and Y. B. Zeldovich. The Observations of Relic Radiation as a Test of the Nature of X-Ray Radiation from the Clusters of Galaxies. *Comments on Astrophysics and Space Physics*, 4:173–+, November 1972.

[43] R. A. Sunyaev and I. B. Zeldovich. Microwave background radiation as a probe of the contemporary structure and history of the universe. ARA&A, 18:537–560, 1980.

[44] J. R. Bond et al. The Sunyaev-Zeldovich effect in CMB-calibrated theories applied to the Cosmic Background Imager anisotropy power at l ¿ 2000. *Astrophys. J.*, 626:12, 2005, astro-ph/0205386.

[45] Eiichiro Komatsu and Uros Seljak. The Sunyaev-Zel'dovich angular power spectrum as a probe of cosmological parameters. *Mon. Not. Roy. Astron. Soc.*, 336:1256, 2002, astro-ph/0205468.

[46] Neelima Sehgal et al. Simulations of the Microwave Sky. *Astrophys. J.*, 709:920–936, 2010, 0908.0540.

[47] N. Battaglia, J. R. Bond, C. Pfrommer, J. L. Sievers, and D. Sijacki. Simulations of the Sunyaev-Zel'dovich Power Spectrum with AGN Feedback. *ArXiv e-prints*, March 2010, 1003.4256.

[48] Richard Kessler et al. First-year Sloan Digital Sky Survey-II (SDSS-II) Supernova Results: Hubble Diagram and Cosmological Parameters. *Astrophys. J. Suppl.*, 185:32–84, 2009, 0908.4274.

[49] Gajus Miknaitis et al. The ESSENCE Supernova Survey: Survey Optimization, Observations, and Supernova Photometry. *Astrophys. J.*, 666:674, 2007, astro-ph/0701043.

[50] W. Michael Wood-Vasey et al. Observational Constraints on the Nature of the Dark Energy: First Cosmological Results from the ESSENCE Supernova Survey. *Astrophys. J.*, 666:694–715, 2007, astro-ph/0701041.

[51] P. Astier, J. Guy, N. Regnault, R. Pain, E. Aubourg, D. Balam, S. Basa, R. G. Carlberg, S. Fabbro, D. Fouchez, I. M. Hook, D. A. Howell, H. Lafoux, J. D. Neill, N. Palanque-Delabrouille, K. Perrett, C. J. Pritchet, J. Rich, M. Sullivan, R. Taillet, G. Aldering, P. Antilogus, V. Arsenijevic, C. Balland, S. Baumont, J. Bronder, H. Courtois, R. S. Ellis, M. Filiol, A. C. Gonçalves, A. Goobar, D. Guide, D. Hardin, V. Lusset, C. Lidman, R. McMahon, M. Mouchet, A. Mourao, S. Perlmutter, P. Ripoche, C. Tao, and N. Walton. The Supernova Legacy Survey: measurement of Ω_M, Ω_Λ and w from the first year data set. A&A, 447:31–48, February 2006, arXiv:astro-ph/0510447.

[52] P. M. Garnavich, R. P. Kirshner, P. Challis, J. Tonry, R. L. Gilliland, R. C. Smith, A. Clocchiatti, A. Diercks, A. V. Filippenko, M. Hamuy, C. J. Hogan, B. Leibundgut, M. M. Phillips, D. Reiss, A. G. Riess, B. P. Schmidt, R. A. Schommer, J. Spyromilio, C. Stubbs, N. B. Suntzeff, and L. Wells. Constraints on Cosmological Models from Hubble Space Telescope Observations of High-z Supernovae. *Astrophys. J., Lett.*, 493:L53+, February 1998, arXiv:astro-ph/9710123.

[53] Robert A. Knop et al. New Constraints on Ω_M, Ω_Λ, and w from an Independent Set of Eleven High-Redshift Supernovae Observed with HST. *Astrophys. J.*, 598:102, 2003, astro-ph/0309368.

[54] A. G. Riess, L.-G. Strolger, J. Tonry, S. Casertano, H. C. Ferguson, B. Mobasher, P. Challis, A. V. Filippenko, S. Jha, W. Li, R. Chornock, R. P. Kirshner, B. Leibundgut, M. Dickinson, M. Livio, M. Giavalisco, C. C. Steidel, T. Benítez, and Z. Tsvetanov. Type Ia Supernova Discoveries at z ¿ 1 from the Hubble Space Telescope: Evidence for Past Deceleration and Constraints on Dark Energy Evolution. ApJ, 607:665–687, June 2004.

[55] A. G. Riess, L.-G. Strolger, S. Casertano, H. C. Ferguson, B. Mobasher, B. Gold, P. J. Challis, A. V. Filippenko, S. Jha, W. Li, J. Tonry, R. Foley, R. P. Kirshner, M. Dickinson, E. MacDonald, D. Eisenstein, M. Livio, J. Younger, C. Xu, T. Dahlén, and D. Stern. New Hubble Space Telescope Discoveries of Type Ia Supernovae at z ¿= 1: Narrowing Constraints on the Early Behavior of Dark Energy. ApJ, 659:98–121, April 2007, arXiv:astro-ph/0611572.

[56] Beth A. Reid et al. Cosmological Constraints from the Clustering of the Sloan Digital Sky Survey DR7 Luminous Red Galaxies. 2009, 0907.1659.

[57] R. Massey et al. COSMOS: Three-dimensional Weak Lensing and the Growth of Structure. ApJS, 172:239–253, September 2007, arXiv:astro-ph/0701480.

[58] J. Lesgourgues, M. Viel, M. G. Haehnelt, and R. Massey. A combined analysis of 3D weak lensing, Lyman-α forest and WMAP year three data. *Journal of Cosmology and Astro-Particle Physics*, 11:8–+, November 2007, arXiv:0705.0533.

[59] H. Hoekstra, Y. Mellier, L. van Waerbeke, E. Semboloni, L. Fu, M. J. Hudson, L. C. Parker, I. Tereno, and K. Benabed. First Cosmic Shear Results from the Canada-France-Hawaii Telescope Wide Synoptic Legacy Survey. ApJ, 647:116–127, August 2006, arXiv:astro-ph/0511089.

[60] C. Schimd, I. Tereno, J.-P. Uzan, Y. Mellier, L. van Waerbeke, E. Semboloni, H. Hoekstra, L. Fu, and A. Riazuelo. Tracking quintessence by cosmic shear. Constraints from

VIRMOS-Descart and CFHTLS and future prospects. A&A, 463:405–421, February 2007, arXiv:astro-ph/0603158.

[61] H. Hoekstra, H. K. C. Yee, M. D. Gladders, L. F. Barrientos, P. B. Hall, and L. Infante. A Measurement of Weak Lensing by Large-Scale Structure in Red-Sequence Cluster Survey Fields. ApJ, 572:55–65, June 2002, arXiv:astro-ph/0202285.

[62] Henk Hoekstra, Howard K. C. Yee, and Mike D. Gladders. Constraints on Omegam and sigma8 from weak lensing in RCS fields. *Astrophys. J.*, 577:595–603, 2002, astro-ph/0204295.

[63] L. Van Waerbeke, Y. Mellier, and H. Hoekstra. Dealing with systematics in cosmic shear studies: New results from the VIRMOS-Descart survey. A&A, 429:75–84, January 2005, arXiv:astro-ph/0406468.

[64] J. Benjamin, C. Heymans, E. Semboloni, L. van Waerbeke, H. Hoekstra, T. Erben, M. D. Gladders, M. Hetterscheidt, Y. Mellier, and H. K. C. Yee. Cosmological constraints from the 100 square degree weak-lensing survey. MNRAS, 381:702–712, October 2007, arXiv:astro-ph/0703570.

[65] S. DeLope Amigo, W. Man-Yin Cheung, Z. Huang, and S.-P. Ng. Cosmological constraints on decaying dark matter. *Journal of Cosmology and Astro-Particle Physics*, 6:5–+, June 2009, 0812.4016.

[66] Z. Huang, J. R. Bond, and L. Kofman. Parameterizing and Measuring Dark Energy Trajectories from Late-Inflatons. *ArXiv e-prints*, July 2010, 1007.5297.

[67] R. E. Smith, J. A. Peacock, A. Jenkins, S. D. M. White, C. S. Frenk, F. R. Pearce, P. A. Thomas, G. Efstathiou, and H. M. P. Couchman. Stable clustering, the halo model and non-linear cosmological power spectra. MNRAS, 341:1311–1332, June 2003, arXiv:astro-ph/0207664.

[68] P. McDonald et al. The Linear Theory Power Spectrum from the Lyα Forest in the Sloan Digital Sky Survey. ApJ, 635:761–783, December 2005, arXiv:astro-ph/0407377.

[69] P. McDonald et al. The Lyα Forest Power Spectrum from the Sloan Digital Sky Survey. ApJS, 163:80–109, March 2006, arXiv:astro-ph/0405013.

[70] Planck Science Team. *Planck: The Scientific Programme (Blue Book). ESA-SCI (2005)-1. Version 2.* European Space Agency., 2009.

[71] Euclid Study Team. *Euclid Assessment study report (SRE-2009-2).* European Space Agency., 2009.

[72] CHIME Science Team. *CHIME Executive Summary.* 2009.

[73] A. Albrecht, G. Bernstein, R. Cahn, W. L. Freedman, J. Hewitt, W. Hu, J. Huth, M. Kamionkowski, E. W. Kolb, L. Knox, J. C. Mather, S. Staggs, and N. B. Suntzeff. Report of the Dark Energy Task Force. *ArXiv Astrophysics e-prints*, September 2006, arXiv:astro-ph/0609591.

[74] Dragan Huterer and Glenn Starkman. Parameterization of dark-energy properties: A principal-component approach. *Phys. Rev. Lett.*, 90:031301, 2003, astro-ph/0207517.

[75] Cora Dvorkin and Wayne Hu. CMB Constraints on Principal Components of the Inflaton Potential. *Phys. Rev.*, D82:043513, 2010, 1007.0215.

[76] Pia Mukherjee, David Parkinson, and Andrew R. Liddle. A nested sampling algorithm for cosmological model selection. *Astrophys. J.*, 638:L51–L54, 2006, astro-ph/0508461.

[77] Andrew R. Liddle, Pia Mukherjee, and David Parkinson. Cosmological model selection. *Astron. Geophys.*, 47:4.30–4.33, 2006, astro-ph/0608184.

[78] Ewan D. Stewart and David H. Lyth. A more accurate analytic calculation of the spectrum of cosmological perturbations produced during inflation. *Phys. Lett.*, B302:171–175, 1993, gr-qc/9302019.

[79] Pascal M. Vaudrevange, Dmitry I. Podolsky, and Glenn D. Starkman. Surprising phenomena in a rich new class of inflationary models. *JCAP*, 1004:031, 2010, 0911.3397.

[80] J. C. Mason and D. C. Handscomb. *Chebyshev Polynomials*. Chapman and Hall/CRC, 2003. p.112.